

國立臺灣大學理學院物理學系

碩士論文

Department of Physics

College of Science

National Taiwan University

Master Thesis



二維易辛模型考慮次近鄰交互作用其相變化及淬火動力學
The Quench Dynamics and the Critical Behavior of the $J_1 - J_2$
Ising Model

郭子傑

Tzu-Chieh Kuo

指導教授：高英哲博士

Advisor: Ying-Jer Kao Ph.D.

中華民國 103 年 7 月

July, 2014

國立臺灣大學碩士學位論文
口試委員會審定書

二維易辛模型考慮次近鄰交互作用其相變化及淬火動力學

The Quench Dynamics and the Critical Behavior of the
 J_1 - J_2 Ising Model

本論文係郭子傑君 (R01222008) 在國立臺灣大學物理學系、所
完成之碩士學位論文，於民國 103 年 7 月 25 日承下列考試委員審查
通過及口試及格，特此證明

口試委員：

高英哲

(簽名)

(指導教授)

陳柏中

林瑜瑛



致謝

首先要感謝高英哲教授三年多以來的指導，這段時間我獲益良多，其中包含學習作業系統、程式語言及物理相關的知識，最重要的是學到如何解決大大小小的問題，並發掘如何使用及學習原本不了解的事物的方法。接著要感謝研究室的同學們，吳柏寬同學、楊淵榮同學及謝昀達學長，在課業、研究及其它大大小小事情上的幫助不勝枚舉，並要感謝羅雅琳、林昇慶、王彥植、周昀萱、蕭維翰、林育平及高文瀚，營造了一個十分良好的氣氛使我在研究室能有快樂的時光，十分讓人感動。還要謝謝杜韋霖、賴昀樅及林法慧於各個方面的協助。此外要感謝其他所有不令我厭惡的人們，他們的存在使我的世界更加美好。最後要感謝我的母親，林思蘭，我成長中最重要的人物，讓我能順利的完成學業。



中文摘要

於圖形處理單元 (GPU) 環境中使用平行演算法及蒙地卡羅演算法模擬了二維方格易辛模型並考慮次近鄰之交互作用，其中最近鄰 (J_1) 與次近鄰 (J_2) 之交互作用皆為反鐵磁性且互為競爭關係，本篇展現了如何計算出臨界指數與交互作用比例 (J_2/J_1) 之關係，及利用 Metropolis 演算法模擬非平衡淬火至臨界溫度並計算出動力學指數。

關鍵字：古典蒙地卡羅演算法、有限尺度效應、圖形處理單元、二維方格易辛模型考慮次近鄰之交互作用、淬火動力學、Kibble-Zurek 機制



Abstract

We perform the Monte Carlo simulations of the $J_1 - J_2$ (frustrated) Ising model on a square lattice with competing coupling $J_1 > 0$ (nearest-neighbor, anti-ferromagnetic) and $J_2 > 0$ (next-nearest neighbor, also anti-ferromagnetic) using the graphic processing unit (GPU). In this thesis, we present the critical exponents evolution as one tunes J_2/J_1 and the extraction of the dynamical exponent using non-equilibrium quenching with Metropolis algorithm to the critical point.

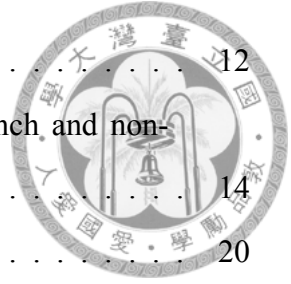
Key words: Classical Monte Carlo, finite-size scaling, GPU, $J_1 - J_2$ Ising model, quench dynamics, Kibble-Zurek mechanism



Contents

口試委員會審定書	i
致謝	ii
中文摘要	iii
Abstract	iv
Contents	v
List of Figures	vii
List of Tables	ix
1 Introduction	1
2 Theory	3
2.1 Ising model on a square lattice	3
2.2 $J_1 - J_2$ Ising model on a square lattice	3
2.3 Monte Carlo simulation	5
2.3.1 Classical Monte Carlo method	5
2.3.2 Metropolis algorithm	7
2.3.3 Parallel tempering Monte Carlo method	7
2.3.4 Calculated observables	8
2.4 Finite-size scaling	10
2.5 Non-equilibrium quenching	12

2.5.1	Kibble-Zurek Mechanism	12
2.5.2	Complete finite-size scaling form with linear quench and non-linear quench	14
2.6	Statistics and data analysis	20
2.7	GPU	22
2.7.1	GPU architecture	22
2.7.2	Algorithm of $J_1 - J_2$ Ising model on GPU	25
3	Results	26
3.1	Critical temperatures and critical exponents	26
3.2	Extraction of the dynamic exponent	36
4	Summary and Discussion	40
	Bibliography	42





List of Figures

2.1	Possible ground states of $J_1 - J_2$ Ising model on a square lattice	4
2.2	Sketch of a rough energy landscape.	7
2.3	Overlap of probability distribution.	8
2.4	Ground states of $J_1 - J_2$ Ising model on a square lattice	9
2.5	Temperature versus Monte Carlo steps with different quench types	16
2.6	$\langle m^2 \rangle$ versus Monte Carlo steps with different quench times	17
2.7	$\langle m^2 \rangle$ versus Monte Carlo steps with different quench size	18
2.8	GPU hardware model	23
2.9	A sample of programming with GPUs	24
2.10	The checkerboard decompositions	25
3.1	Binder cumulants versus temperatures for the first-order and continuous phase transitions	27
3.2	$\delta U / \delta K$ versus temperature	28
3.3	Maximums of $\delta U / \delta K$, $\delta \ln M / \delta K$ and $\delta \ln M / \delta K$	28
3.4	Specific heat versus temperature for the first-order transition	29
3.5	Specific heat versus temperature for continuous phase transition	30
3.6	Magnetization versus temperature	31
3.7	Susceptibility versus temperature	31
3.8	Pseudo critical temperatures of each quantities	32
3.9	Critical temperatures for $0 \leq g \leq 1.5$	33
3.10	The maximum values of each quantities	33
3.11	ν for $0 \leq g \leq 1.5$	34

3.12	α for $0 \leq g \leq 1.5$	34
3.13	β for $0 \leq g \leq 1.5$	35
3.14	γ for $0 \leq g \leq 1.5$	35
3.15	$\langle m^2 \rangle L^{2\beta/\nu}$ versus $vL^{zr+1/\nu}$	37
3.16	$\langle m^2 \rangle L^2$ versus v^{-1}	38
3.17	z for $0 \leq g \leq 1.5$	39





List of Tables

3.1	The dynamic exponents from references.	39
-----	--	----



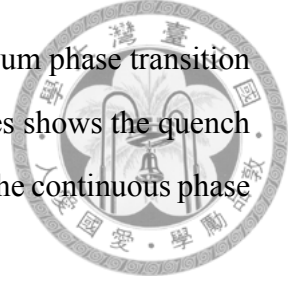
Chapter 1

Introduction

The Ising model on a two dimensional (2D) square lattice is a rare example, which can be solved exactly, so we can compute the quantities at any temperature. This allows the calculation of the critical exponents of the continuous phase transition between the ferromagnetic phase and the disorder state. Adding a competing interaction on the next-nearest-neighbor sites provides new phases and new types of phase transition different from the Ising universality class in some cases. In the 2D $J_1 - J_2$ Ising model, when the ratio of interaction $g = J_2/J_1 < 1/2$, there is an Ising-like transition [1–10]. There is a new striped phase which is with alternating stripes of positive and negative magnetization oriented in either the x or the y direction when $g > 1/2$, the ordering breaks a four-fold Z_4 symmetry as the temperature increases. Unlike the Ising transition with Z_2 symmetry, the phase transition between the Z_4 -ordered state and disordered state can not be described simply by the symmetry of the order parameter so it cannot be solved exactly. The critical exponents may vary with the ratio g and only ratios of the exponents are fixed at different g . Some recent studies have found that there is a continuous transition which can be mapped to Ashkin-Teller (AT) model for $g > g^*$, a weak first-order phase transition for $1/2 < g \leq g^*$ and a Potts transition point at $g = g^*$ where $g^* \approx 0.67$ [1–4].

The above paragraph is based on the theories which analyze the equilibrium states, but what we are also interested in is a system in a non-equilibrium state, especially the dynamics of a quenching system. Based on the renormalization group (RG) theory, the theories of the finite-size scaling used to analyze the equilibrium states are established

[11–13]. The scaling hypotheses are also generalized to non-equilibrium phase transition and the dynamic critical behavior [12, 14–19]. Some recent researches shows the quench dynamics of the classical Ising transition [14, 20], and we extend it to the continuous phase transitions regimes in the $J_1 - J_2$ Ising model.



In this thesis, we present some evidences to support the types of the transitions mentioned in the first paragraph using Monte Carlo (MC) simulation, especially the critical exponents. In addition, we focus on the non-equilibrium quenching to the critical temperature T_c with Metropolis algorithm. Then we extract the dynamic exponent z considering linear and non-linear quenches for different transitions.

We organize the thesis in following ways: In Ch. 2, we summarize some known scenarios of the $J_1 - J_2$ Ising model and the theories used to do the simulations and the analyses. We then investigate the phase transitions and the quench dynamics of the $J_1 - J_2$ Ising model in Ch. 3. Finally, we give a brief conclusion of the results in Ch. 4.



Chapter 2

Theory

2.1 Ising model on a square lattice

Consider a classical magnetic system, an easy example is the Ising model. The Ising model on a square lattice is defined by the hamiltonian

$$H = J \sum_{\langle i,j \rangle} \sigma_i \sigma_j - h \sum_i \sigma_i, \quad (2.1)$$

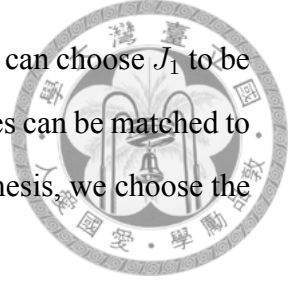
where $J < 0$ (ferromagnetic), $\langle i, j \rangle$ denotes the nearest-neighbors on the square lattice, h is a uniform external magnetic field, and the spin variables $\sigma_i, \sigma_j = \pm 1$ which point up or down on the easy axis. The term $-h \sum_i \sigma_i$ describes the Zeeman energy of the system, which we do not focus on in this thesis. Note that the Ising model on a 2D square lattice can be solved exactly, so it can be a start of studying the phase transition.

2.2 $J_1 - J_2$ Ising model on a square lattice

The 2D $J_1 - J_2$ Ising model, also called frustrated Ising model, is defined by the hamiltonian

$$H = J_1 \sum_{\langle i,j \rangle} \sigma_i \sigma_j + J_2 \sum_{\langle\langle i,j \rangle\rangle} \sigma_i \sigma_j, \quad (2.2)$$

where $\langle i, j \rangle$ and $\langle\langle i, j \rangle\rangle$ denotes first and second (diagonal) neighbors on the square lattice, and the spin variables $\sigma_i, \sigma_j = \pm 1$. To make the couplings compete to each other, we



have two choices. First, let J_2 be positive (antiferromagnetic), and we can choose J_1 to be positive (antiferromagnetic) or negative(ferromagnetic). The two cases can be matched to each other easily by changing all the signs of one sublattice. In this thesis, we choose the first case.

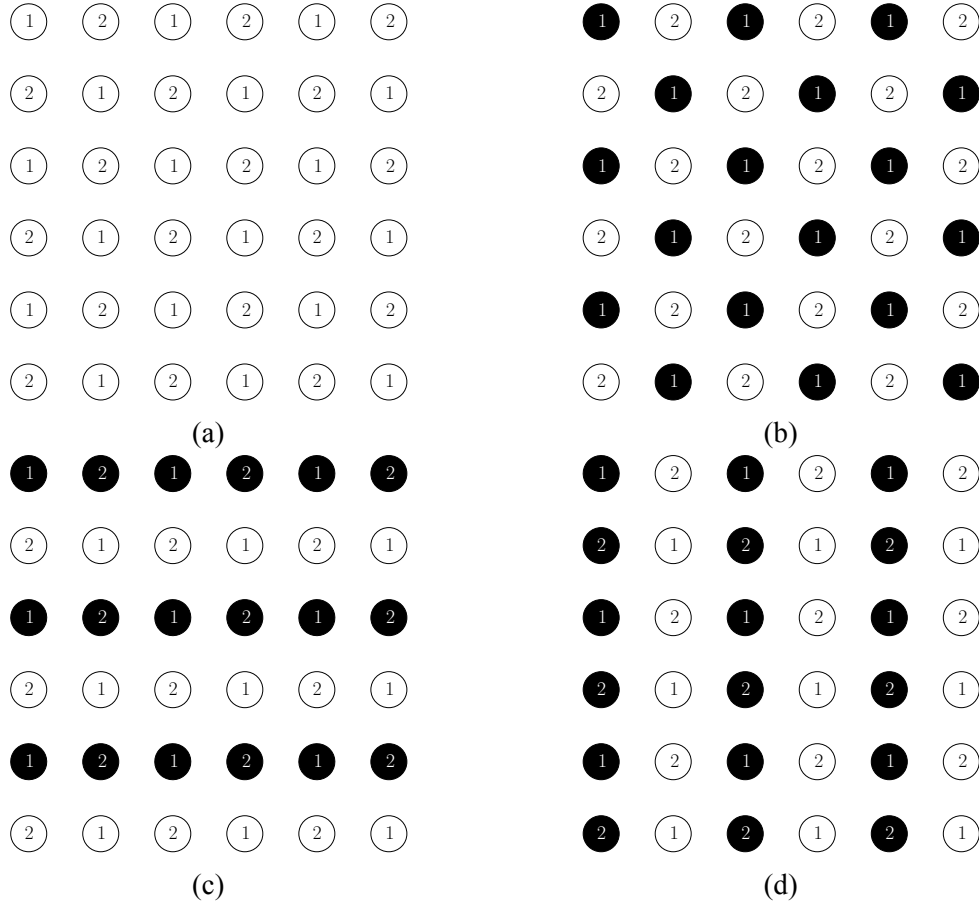


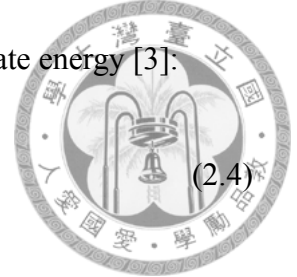
Figure 2.1: The black circles represent spins up and the white circles represent spins down. If J_1 is negative and $|g| < 0.5$, the ground state is ferromagnetic (shown in (a)); if J_1 is positive and $|g| < 0.5$, the ground state is antiferromagnetic, also called as Néel state (shown in (b)); if $|g| > 0.5$, the ground state is the striped state (shown in (c)(d)). Changing the sign of J_1 means changing the signs of all spins in sublattice 1 or 2. Examples are shown as those from left to right or from right to left. It make the ground state from ferromagnetic to antiferromagnetic for $|g| < 0.5$, and no specific change for $|g| > 0.5$.

When the ratio $g = J_2/J_1 < 1/2$, there is an Ising-like transition to a Néel state with the ground state energy (per site) [1–10]:

$$E_{Néel} = -2(J_1 - J_2). \tag{2.3}$$

And the ground state for $g > 1/2$ is a stripe phase with the ground state energy [3].

$$E_{\text{stripe}} = -2J_2. \quad (2.4)$$



Recent researches show that there is a very weak first-order transition for $1/2 < g < g^*$ with $g^* \approx 0.67$. For $g \geq g^*$ it is a continuous transition which can be mapped into the Ashkin-Teller (AT) model, it back to be an Ising-like (2-state Potts) transition as $g \rightarrow \infty$, and there is a Potts transition point at $g = g^*$ [1, 2]. It is also an interesting point for $g = 1/2$, the critical temperature seems to close to 0 at this point. [3, 8–10]

2.3 Monte Carlo simulation

2.3.1 Classical Monte Carlo method

The Monte-Carlo method is an algorithm to simulate a thermal ensemble [12, 21–23]. Consider a system in state s . In the canonical ensemble with temperature T , the probability of the state s with energy E is denoted by $e^{-\beta E}$, where $\beta = 1/kT$. The partition function of the canonical ensemble is given by

$$Z = \sum_s e^{-\beta H(s)}, \quad (2.5)$$

which sums over all possible states of the system. Here $H(s)$ is the Hamiltonian of the system at state s . And the thermodynamic average of a physical quantity is given by

$$\langle O \rangle = \frac{1}{Z} \sum_s e^{-\beta H(s)} O(s). \quad (2.6)$$

It is hard to sum over all states of the system since the number of micro-states is too large for a reasonable system size. For instance, an Ising model of N spins with only two spin configurations ± 1 , the total number of states is 2^N . So we should use a better way to do the sample the configurations and replace the ensemble average by a time average. Suppose we have a probability distribution of each states $W(s)$ when we are doing the

sampling, and the average becomes

$$\begin{aligned}\langle O \rangle &= \frac{\sum_s e^{-\beta H(s)} O(s)}{\sum_s e^{-\beta H(s)}} \\ &= \frac{\sum_s e^{-\beta H(s)} O(s) / W(s)}{\sum_s e^{-\beta H(s)} / W(s)}.\end{aligned}\tag{2.7}$$



The simplest choice for $W(s)$ in Eq. (2.7) is $W(s) \sim e^{-\beta H(s)}$, and the Boltzmann factor cancels out, Eq. (2.7) reduces to

$$\langle O \rangle = \frac{1}{M} \sum_s O(s),\tag{2.8}$$

where M is total number of micro-states. This method is also called the importance sampling. Now we need generate a sequence of states $s_1 \rightarrow s_2 \rightarrow \dots \rightarrow s_i \rightarrow s_{i+1} \rightarrow \dots$, with initial state s_1 , and a series of “warm up” steps, reach a steady sequence of the equilibrium states from the n -th step. The time average of the equilibrium sequence should be equal to the ensemble average of a canonical ensemble. So the objective is to construct a Markov process with transition probability $P(s_1|s_2)$ for $s_1 \rightarrow s_2$ to satisfy the equilibrium probability distribution

$$W_{eq}(s) = \frac{e^{-\beta H(s)}}{z}.\tag{2.9}$$

To find the conditional probability, we apply the following limitations:

$$P(s_i|s_f) \geq 0,\tag{2.10a}$$

$$\sum_{s_f} P(s_i|s_f) = 1,\tag{2.10b}$$

$$W_{eq}(s_i)P(s_i|s_f) = W_{eq}(s_f)P(s_f|s_i).\tag{2.10c}$$

The first two are the basic properties of probability. The last one is imposed by the principle of detail balance.



2.3.2 Metropolis algorithm

One of the convenient choice for $P(s_i|s_f)$ is the Metropolis (also known as Metropolis-Hastings) algorithm [12, 21–23]. It goes as following:

1. Pick a random site α .
2. Compute the energy change $\Delta H = H(s_f) - H(s_i)$ if the spin at site α flipped.
3. Flip the spin if $\Delta H \leq 0$; flip it with probability $e^{-\beta\Delta H}$ if $\Delta H > 0$.
4. Repeat 1 to 3 until all the sites are checked.

Finish the above procedure once is called a Monte Carlo step (MCS). And one can check the probability distribution easily by taking the probability into (2.10c).

2.3.3 Parallel tempering Monte Carlo method

The Metropolis algorithm can reach the correct probability distribution of the states after equilibration. But to reach the equilibrium would need a large number of sweeps for a system which is head to equilibrate. Unfortunately, the $J_1 - J_2$ Ising model perform hard to reach equilibrium when g is near $1/2$. So we need another tool to help us do the simulations. A powerful way is called the parallel temping [21, 23, 24].

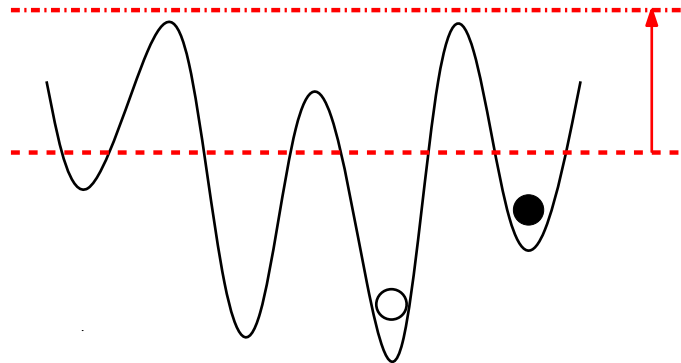


Figure 2.2: Sketch of a rough energy landscape. If a system at T_1 is trapped in a local minimum but not at T_2 . The system at T_1 moves from initial state (solid circle, local minimum), is hard to reach the final state (global minimum, open circle) with the simple MC simulations. But the system at T_1 is more likely to climb up the barrier and reaches the global minimum with the help of parallel tempering.

M non-interacting copies of the system are simulated in parallel at different temperatures $\{T_1, T_2, \dots, T_M\}$ where the temperature set is sorted as $T_i < T_{i+1}$ for convenience.

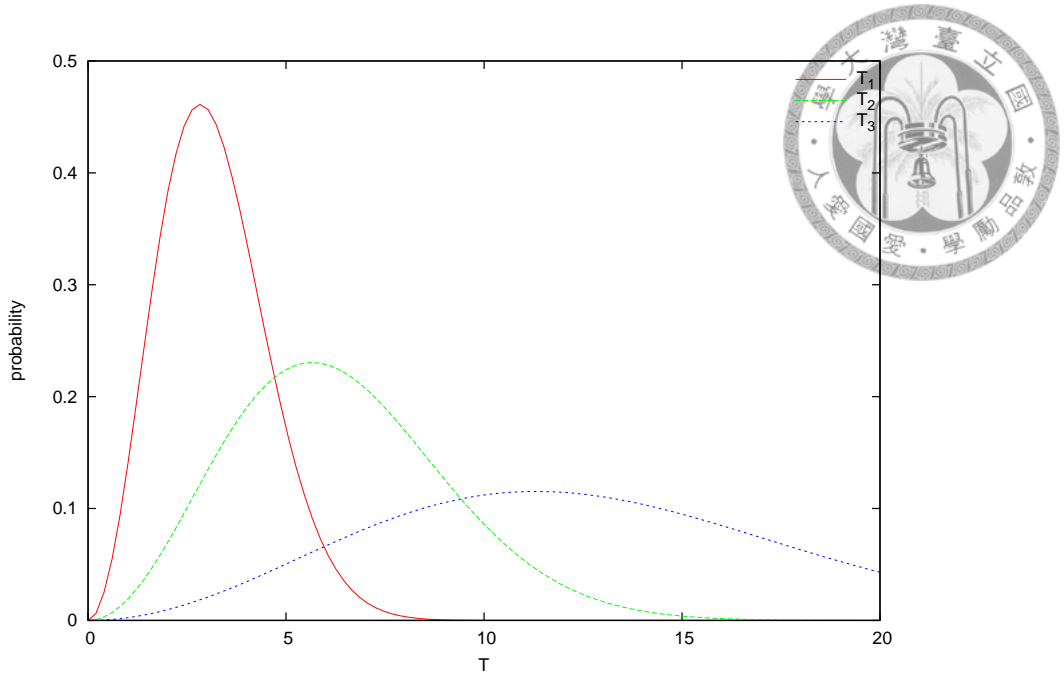


Figure 2.3: Figure shows the probability distribution of system at 3 different temperatures, where $T_1 < T_2 < T_3$. The overlap is bigger if ΔT is smaller. If ΔT is too small, it may decrease the efficiencies of the simulations; if ΔT is too large, the overlap is too small to do the tempering.

After a fixed number of Monte-Carlo sweeps, two copies of neighboring temperatures T_i and T_{i+1} are exchanged with a acceptance probability

$$p = \min\{1, e^{(E_{i+1}-E_i)(\beta_{i+1}-\beta_i)}\}. \quad (2.11)$$

Note that the exchanging probability also satisfy the detail balance. The Metropolis algorithm is very inefficient when a configuration is trapped in a local minimum of energy, the tempering can help it explore the energy landscape easily. Usually we choose the temperature set where the acceptance probabilities are approximately independent of temperatures and between approximately 20%-80%.

2.3.4 Calculated observables

Before we go into the details, we define the observables measured in the MC simulations for the $J_1 - J_2$ model first.

Since the $J_1 - J_2$ model we discussed is not in a ferromagnetic state, magnetization is not a good order parameter. To distinguish the ordered phase and disordered phase. Let

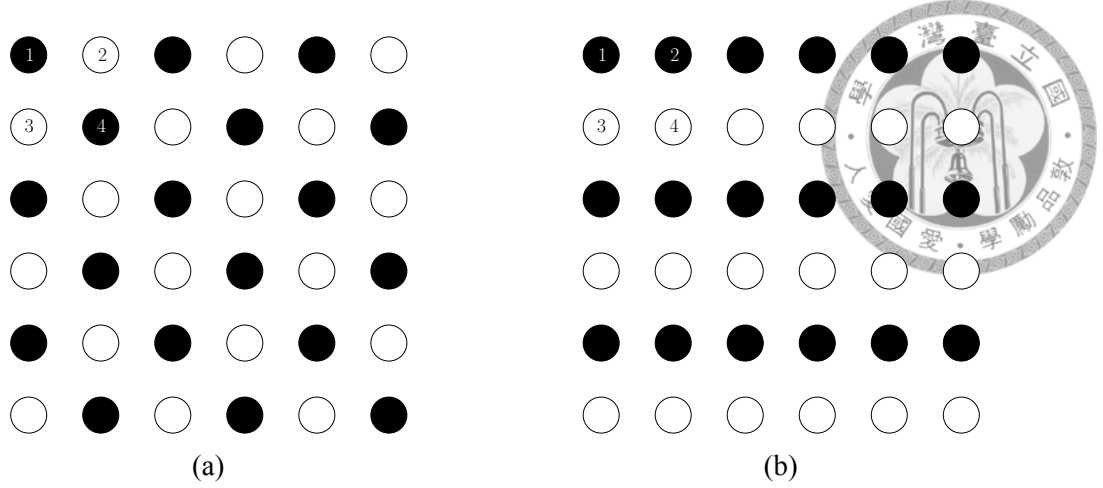


Figure 2.4: Fig. (a) shows the Néel state for $g < 0.5$. Fig. (b) show the striped states for $g < 0.5$ in horizontal direction. One can easily define the order parameters of each by split them into lattices with size 2 by 2. For example, $M_{Néel} = (M_1 - M_2 + M_3 - M_4)/4$ in (a) and $M_y = (M_1 + M_2 - M_3 - M_4)/4$ in (b) where M_i is the average of the spins at corner i of each 2 by 2 lattice.

us define the order parameters of both ground states. In Fig 2.4, one can define the order parameters simply, just sum the spins in different sublattice timed different by a factor -1 .

For the Néel state, the order parameter is defined as

$$M_{Néel} = \frac{1}{N} \sum_{i=1}^N \sigma_i (-1)^{x_i + y_i}, \quad (2.12)$$

where (x_i, y_i) are the coordinates of site i , L is the size of the 2D periodic lattice and $N = L^2$ is the number of spins. For the striped phase, we can define two components of the order parameter in two directions

$$M_x = \frac{1}{N} \sum_{i=1}^N \sigma_i (-1)^{x_i}, \quad (2.13a)$$

$$M_y = \frac{1}{N} \sum_{i=1}^N \sigma_i (-1)^{y_i}, \quad (2.13b)$$

with a root-mean-square order parameter

$$M_{rms} = \sqrt{M_x^2 + m_y^2}. \quad (2.14)$$

By definition of the order parameters, we define the susceptibility as

$$\chi = \frac{d\langle M \rangle}{dh} = \frac{N}{T} (\langle M^2 \rangle - \langle |M| \rangle^2), \quad (2.15)$$



where h is the strength of a field coupling to the order parameter, and M is M_{Neel} or M_{rms} for each ground states. We also calculate the fourth order Binder cumulant [11, 25, 26]

$$U = \frac{n+2}{2} \left(1 - \frac{n}{n+2} \frac{\langle M^4 \rangle}{\langle M^2 \rangle^2} \right), \quad (2.16)$$

where n is the number of the components for the order parameter. In this case, $n = 1$ for the Néel order, and $n = 2$ for the striped order. And the factors are chosen to make U be a step function where $U \rightarrow 0$ in the disordered state and $U \rightarrow 1$ in the ordered state. Also, we measure the specific heat

$$C_v = \frac{dE}{dT} = \frac{N}{T^2} (\langle E^2 \rangle - \langle |E| \rangle^2), \quad (2.17)$$

where E is energy per site.

2.4 Finite-size scaling

To discuss finite-size scaling [11–13, 21, 27], first we have to introduce some basic ideas. In an infinite system, the correlation length diverges near the critical temperature as

$$\xi \sim |t|^{-\nu}, \quad (2.18)$$

where $t = \frac{T-T_c}{T_c}$, is the reduced temperature. Note that if the system size $L \gg \xi$, the system is finite but irrelevant and can be regarded as an infinite. If $L \ll \xi$, then L is the

most relevant length-scale. Other observables also have the power-law dependence:

$$C_v \sim |t|^{-\alpha}, \quad (2.19a)$$

$$M \sim |t|^\beta, \quad (2.19b)$$

$$\chi \sim |t|^{-\gamma}. \quad (2.19c)$$



Consider a quantity Q which have a power-law divergence at T_c ,

$$Q \sim |t|^{-\kappa}. \quad (2.20)$$

We also have t as a function of ξ by Eq. (2.18):

$$|t| \sim \xi^{-1/\nu}, \quad (2.21)$$

then Q can be rewrote as

$$Q \sim \xi^{\kappa/\nu}. \quad (2.22)$$

Note that this from is applied for $\xi \ll L$. Since we cannot do the simulation of the infinite size, when $\xi \approx L$, the divergence is no longer continue on the finite size. The critical value of the quantity can be reached at the pseudo critical point when

$$|t_c(L)| \sim L^{-1/\nu}, \quad (2.23)$$

and the critical value of the quantity (maximum or other distinguishable feature) is given by [28]

$$Q_c(L) \sim L^{\kappa/\nu}. \quad (2.24)$$

The hypothesis is that the quantity is also controlled by a non-singular function of the ratio ξ/L , so that the quantity is expressed as

$$Q(t, L) = L^{\kappa/\nu} f(\xi/L), \quad (2.25)$$

with (2.18), we can write as

$$Q(t, L) = L^{\kappa/\nu} g(tL^{1/\nu}), \quad (2.26)$$



From (2.20) we get the above function form. Take (2.19) into (2.20), then we get

$$C_v = L^{\alpha/\nu} \tilde{C}(tL^{1/\nu}), \quad (2.27a)$$

$$M = L^{-\beta/\nu} \tilde{M}(tL^{1/\nu}), \quad (2.27b)$$

$$\chi = L^{\gamma/\nu} \tilde{\chi}(tL^{1/\nu}). \quad (2.27c)$$

Note that the functions above are only valid for T is closed to T_c .

The scaling relations of exponents also had been found using other method (most completed by Fisher, Widom, Rushbrook and Josephson) [13, 27]

$$\alpha + 2\beta + \gamma = 2, \quad (2.28a)$$

$$\nu d = 2 - \alpha, \quad (2.28b)$$

$$\gamma = \nu(2 - \eta) = \beta(\delta - 1), \quad (2.28c)$$

where d is the dimension of the system. These relations are helpful for checking numerical calculation of the exponents, and one can use these relations to calculate other exponents with two or three know exponents.

2.5 Non-equilibrium quenching

2.5.1 Kibble-Zurek Mechanism

The Kibble-Zurek (KZ) argument [29, 30] originally focus on the defect problem and its extensions expand to include the rate of change of quantities of the system. The KZ mechanism and its extensions are successfully used to describe the out-of-equilibrium physics of phase transitions. [12, 14–19]

Consider a system with critical temperature T_c and make the system be quenched from an initial temperature T_i to some final temperature $T_c < T < T_i$. If the quench velocity is sufficiently slow, the system evolves adiabatically to its equilibrium state at temperature T . Else if quench velocity is so high that the system has lots of defects and the adiabatic description breaks down. The KZ mechanism can be used to distinguish these regimes.

The following arguments are based on Ref. [14], and one can see Refs. [17–19] for a general review. According to the arguments of KZ, in quasi-adiabatic regime, the total quench time τ_q must be at least the order of the relaxation time τ_{rel} . The relaxation time is related to the equilibrium spatial correlation length ξ_T .

$$\tau_{rel} \sim \xi_T^z, \quad (2.29)$$

where z is the dynamic exponent. The dynamic exponent z is depend on the equilibrium universality class of phase transition and the stochastic dynamics imposed on the system. So the total quench time related to the velocity v for a linear quench is expressed by

$$\tau_q \sim |T_i - T|/v \sim \tau_{rel} \sim \xi_T^z \sim |T - T_c|^{-z\nu}, \quad (2.30)$$

where ν is the equilibrium correlation length exponent. The remaining time τ is defined as the time from T to critical temperature T_c if the quench is continue. The relation is described as

$$\tau = |T_i - T|/v \sim |T - T_c|^{-z\nu}. \quad (2.31)$$

From the above relation one can define the KZ velocity

$$v_{KZ}(T) \sim |T - T_c|^{1+z\nu}, \quad (2.32)$$

at which the system falls out the adiabatic regime at temperature T .

We also define the correlation length associated with a velocity ξ_v , which is the correlation length reached at a freezing infinite system for a non-equilibrium state. Since

$\xi_v \sim \xi_T$ for the quasi-adiabatic evolution and $\xi_T \sim |T - T_c|^{-\nu}$ at freezing point, we have

$$\xi_v \sim v^{-1/(z+1/\nu)}. \quad (2.33)$$



For a finite system the length scale has maximum L , which means $\xi_v \leq L$. The velocity which separate the adiabatic and non-adiabatic regime can be get by replacing ξ_v by L according to the finite-size scaling theory. The size-dependent KZ velocity is given by

$$v_{KZ}(L) \sim L^{-(z+1/\nu)}. \quad (2.34)$$

For $v < v_{KZ}(L)$, the system is in quasi-adiabatic regime; for $v > v_{KZ}(L)$, the quasi-adiabaticity breaks down.

Here we combine the original finite-size scaling and the KZ mechanism. Adding a velocity ratio v/v_{KZ} into the original scaling function then we have the generalize KZ finite-size scaling;

$$\begin{aligned} Q(t, L, v) &= L^{\kappa/\nu} f'(L/\xi_T, v/v_{KZ}) \\ &= L^{\kappa/\nu} g'(tL^{1/\nu}, vL^{(z+1/\nu)}). \end{aligned} \quad (2.35)$$

2.5.2 Complete finite-size scaling form with linear quench and non-linear quench

To consider the case of the non-linear quench, where the critical point is approached according to a power-law of time t with total time τ_q and final temperature T_c ,

$$T - T_c = v(\tau_q - t)^r, \quad (2.36)$$

where v is the velocity. r describe the quench type, for example, $r = 1$ for a linear quench, $r = 2$ for a quadratic quench and $r = 0$ for a sudden quench. In this thesis, we use $T_i = 1.5T_c$ and express v in units of T_c , so the velocity is described as

$$v = (T_i - T_c)/\tau_q^r \Rightarrow 0.5/\tau_q^r, \quad (2.37)$$

where τ_q is the total quench time. When using Metropolis algorithm, time is in units of Monte-Carlo step.

We also extend the non-linear quench to the other quantities by replacing z by zr . The KZ velocity considering the non-linear quench is expressed as

$$v_{KZ}(L) \sim L^{-(zr+1/\nu)}. \quad (2.38)$$

And the generalized KZ finite-size scaling now described as

$$Q(t, L, v) = L^{\kappa/\nu} g'(tL^{1/\nu}, vL^{(zr+1/\nu)}). \quad (2.39)$$

Consider the case $t = 0$ ($T = T_c$),

$$Q(t = 0, L, v) = L^{\kappa/\nu} g'(vL^{zr+1/\nu}). \quad (2.40)$$

The square of the order parameter shown in Fig 2.6, which is the main quantity studied in the quench part of this thesis;

$$m^2 = \left(\frac{1}{N} \sum_{i=1}^N \sigma_i \right)^2. \quad (2.41)$$

Replace κ by -2β in Eq. (2.39) and the scaling function at T_c is expressed as

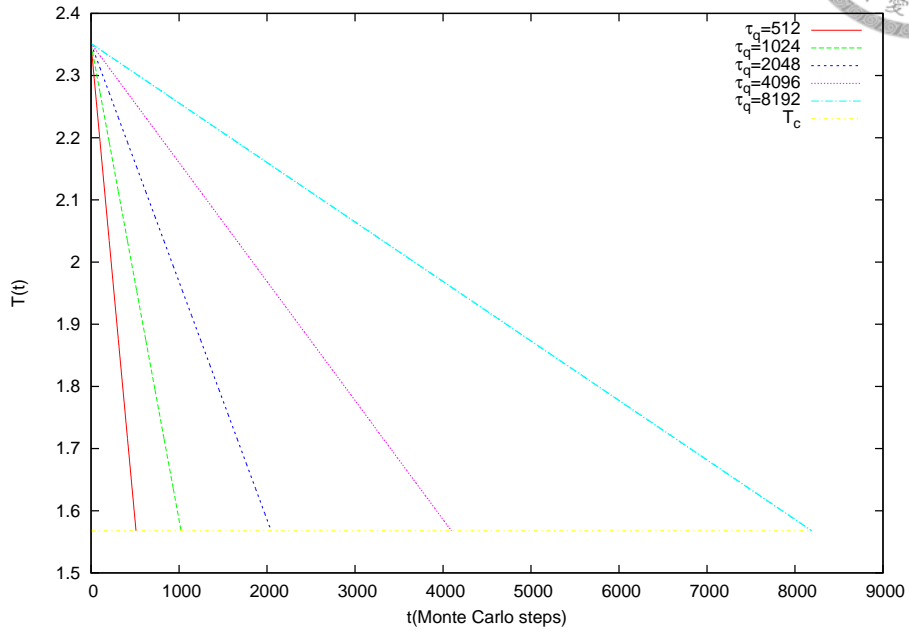
$$\langle m^2 \rangle = L^{-2\beta/\nu} F(vL^{zr+1/\nu}). \quad (2.42)$$

When the quench velocity is very high and the simulated size is large enough (shown in Fig. 2.7), i.e. the KZ correlation length ξ_v is much smaller than L , one expect

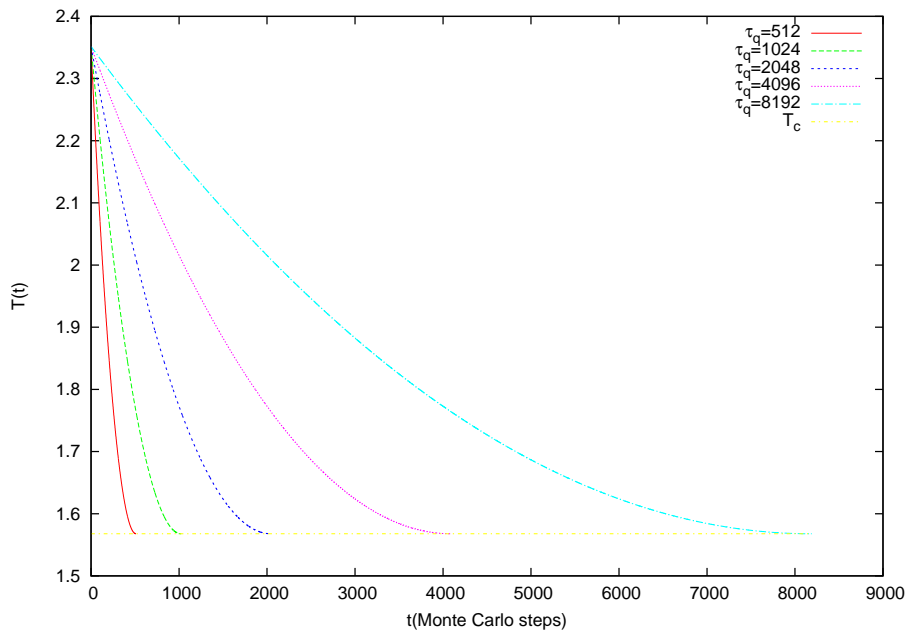
$$\langle m^2 \rangle = \frac{1}{N^2} \sum_i \sum_j \langle \sigma_i \sigma_j \rangle = \frac{1}{N} \sum_i \sum_j \langle \sigma_0 \sigma_j \rangle \sim L^{-d}, \quad (2.43)$$

where d is the number of dimensions; $d = 2$ for the $J_1 - J_2$ model in a square lattice. With



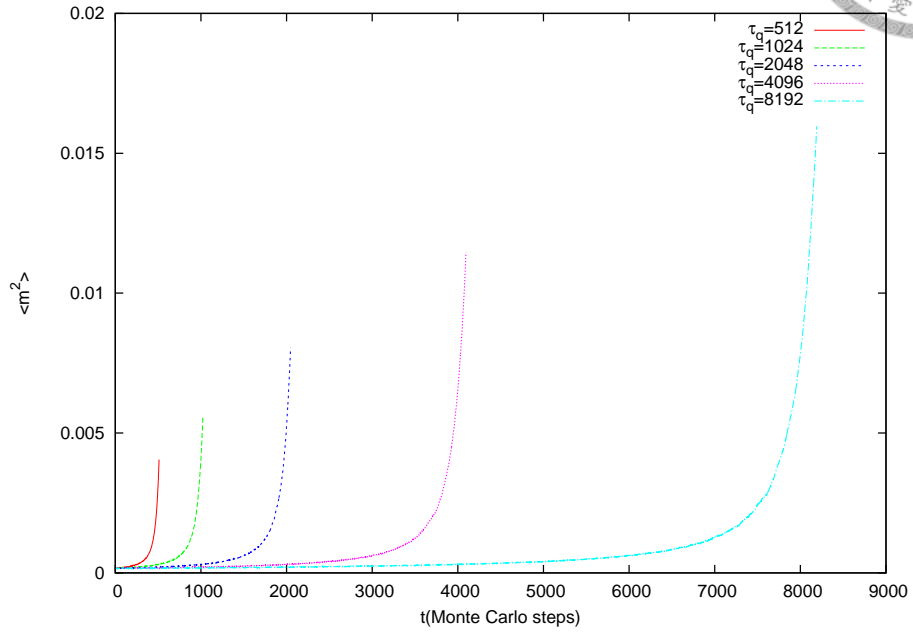


(a) Linear quench with $r = 1$.

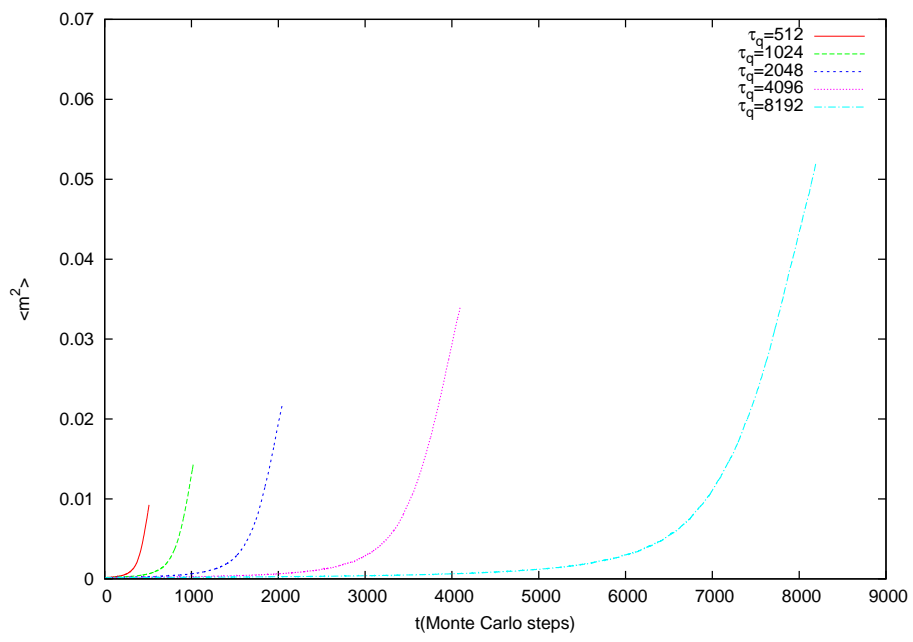


(b) Non-linear quench with $r = 2$.

Figure 2.5: Figure shows temperature versus Monte Carlo steps of a system quenches start at $T_i = 1.5T_c$ and end at T_c with different r for $g = 0.8$.

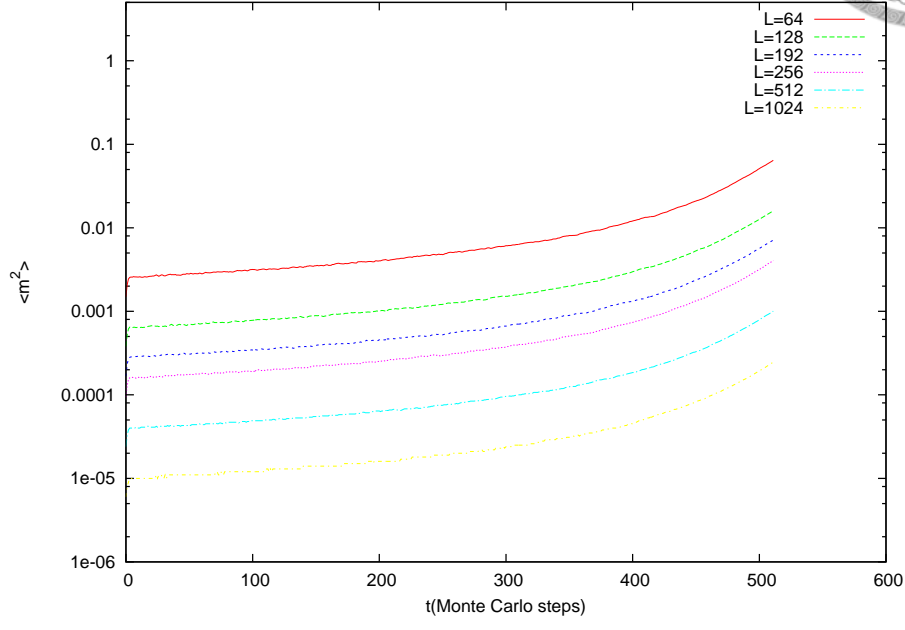


(a) Linear quench with $r = 1$.

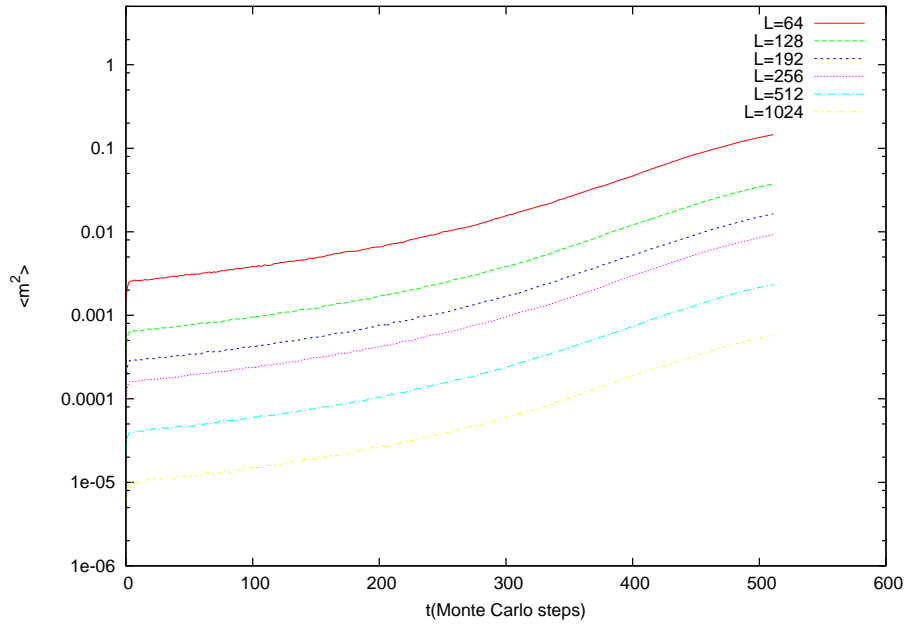


(b) Non-linear quench with $r = 2$.

Figure 2.6: Figure shows $\langle m^2 \rangle$ changes as function of time of a system quenches start at $T_i = 1.5T_c$ and end at T_c with different r for $g = 0.8$ and simulated size $L = 256$.



(a) Linear quench with $r = 1$.



(b) Non-linear quench with $r = 2$.

Figure 2.7: Figure shows $\langle m^2 \rangle$ versus time of a system quenches start at $T_i = 1.5T_c$ and end at T_c with different r for $g = 0.8$. One can easily find that the L^{-d} dependence.

the scaling form in Eq. (2.42), the function F is reduced to a power law of $vL^{zr+1/\nu}$:

$$\langle m^2 \rangle \sim L^{-2\beta/\nu} (vL^{zr+1/\nu})^{-x}, \quad (2.44)$$

and this exponent x is obtain easily by the function being proportional to L^{-d} , i.e.,

$$x = \frac{d - 2\beta/\nu}{zr + 1/\nu}. \quad (2.45)$$

So there is an intermediate universal scaling regime where

$$\langle m^2 \rangle \sim L^{-d} v^{-x}. \quad (2.46)$$

Note the relation above is not consistent with the sufficient high velocity. For a sufficient high quench velocity, $\langle m^2 \rangle$ still converge to L^{-d} and depend on v . If v reach ultimate high velocity, the dependence of v is dropped out. On the contrast, is the velocity is low enough, Eq. (2.42) tends to the standard finite-size behaviour;

$$\langle m^2 \rangle \sim L^{-2\beta/\nu}, \quad (2.47)$$

Then the scaling function's form of $\langle m^2 \rangle$ is expressed and classified by three regimes:

$$\langle m^2 \rangle = \begin{cases} L^{-2\beta/\nu} \sum_n c_n (vL^{zr+1/\nu})^n, & v \lesssim v_{KZ}(L) \\ L^{-d} c v^{-x}, & v_{KZ}(L) \ll v \ll 1 \\ L^{-d} \sum_n c_n (\frac{1}{v})^n, & v \gtrsim 1, \end{cases} \quad (2.48)$$

The velocity regime $v \lesssim v_{KZ}(L)$ is called the quasi-adiabatic regime, $v_{KZ}(L) \ll v \ll 1$ is called the universal scaling regime and $v \gtrsim 1$ is called the diabatic regime. In this thesis we focuses on the universal scaling regime.

2.6 Statistics and data analysis



To extract the scaling function g in Eq. (2.26), one can use data collapsing [11, 12]

We define

$$x_L = tL^{1/\nu}, \quad (2.49a)$$

$$y_L = Q(t, L)L^{-\kappa/\nu}, \quad (2.49b)$$

and plot y_L versus x_L for different temperature T and different system size L , if the hypothesis is correct, all of the data should collapse to same curve, which is the scaling function, $g(x) = y_{L \rightarrow \infty}(x)$. Given a set of parameters T_c , ν and κ , we have a set of data points (x_L, y_L) . A high-order polynomial is used to fit the scaling function. To find the best set from the sets of parameters, we use the reduced-chi-square χ_{red}^2 to express the goodness of the fit. The χ_{red}^2 is defined as

$$\chi_{red}^2 = \frac{1}{n - p - 1} \sum_{i=1}^n \frac{(f(x_i) - y_i)^2}{\sigma_i^2}, \quad (2.50)$$

where n is the number of the fitting points, p is the number of fitted parameters and σ_i^2 is the y-variance of the data point (x_i, y_i) . And the statistical variance σ_i^2 is defined as

$$\begin{aligned} \sigma_i^2 &= \frac{1}{n} \sum_{j=1}^n (y_{ij} - \bar{y}_i)^2 \\ &= \langle y_i^2 \rangle - \langle y_i \rangle^2. \end{aligned} \quad (2.51)$$

where the y_{ij} is the j -th y -value for x_i . Note that σ is called the standard deviation. We also define the statistical error SE :

$$SE = \frac{\sigma}{\sqrt{n - 1}}. \quad (2.52)$$

To find the best set of parameters, one should tend to minimize χ_{res} and let it be closed to 1 [11].

But the data collapsing is not always the best way to find the critical exponents and

critical temperature, so we introduce the another methods to find the critical temperature and the critical exponents.

Besides ξ/L , there is also other dimensionless quantities that is useful to extract T_c independently of the critical exponents. The most common one is the Binder ratio [11, 25, 26]:

$$R_2 = \frac{\langle M^4 \rangle}{\langle M^2 \rangle^2} = \tilde{R}_2(tL^{1/\nu}), \quad (2.53)$$

which can compose the Binder cumulant in (2.16). One can also define other ratios similar to (2.53), e.g., $R_1 = \langle M^2 \rangle / \langle |M| \rangle^2$ and $R_E = \langle E^4 \rangle / \langle E^2 \rangle^2$. (Usually R_E is used to find the critical temperature in first-order transition.)

One can also extract a single exponent ν without measuring correlation length ξ , we can start from (2.27b).

$$\begin{aligned} \frac{\delta \ln M}{\delta K} &= \frac{\delta \ln M}{\delta M} \frac{\delta x_t}{\delta K} \frac{\delta M}{\delta x_t} \\ &= \frac{1}{M} \frac{(-K_c L^{1/\nu})}{K^2} \frac{\delta M}{\delta x_t} \\ &\approx L^{1/\nu} F(tL^{1/\nu}) \end{aligned} \quad (2.54)$$

where $K = 1/T$, $x_t = tL^{1/\nu}$ and F is a new scaling function. The condition is that $T \rightarrow T_c$, so that $K^2 \approx K_c^2 \approx const..$ From above equations and extend to another quantity, we have [21, 24, 28, 31, 32]

$$\left(\frac{\delta \ln M}{\delta K} \right)_{max} \sim L^{1/\nu}, \quad (2.55a)$$

$$\left(\frac{\delta \ln M^2}{\delta K} \right)_{max} \sim L^{1/\nu}, \quad (2.55b)$$

$$\left(\frac{\delta U}{\delta K} \right)_{max} \sim L^{1/\nu}. \quad (2.55c)$$

To calculate the above quantities, we may need the help of

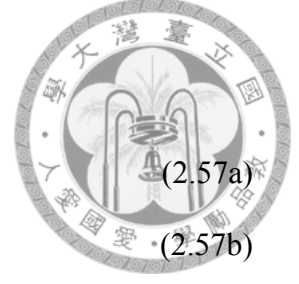
$$\frac{\delta M}{\delta K} = \langle M \rangle \langle E \rangle - \langle ME \rangle. \quad (2.56)$$

Take $T = T_c$ ($t = 0$) in Eq. (2.27),

$$(C_v)_c \sim L^{\alpha/\nu}, \quad (2.57a)$$

$$M_c \sim L^{-\beta/\nu}, \quad (2.57b)$$

$$\chi_c \sim L^{\gamma/\nu}. \quad (2.57c)$$



The above equations are not applicable to the case which T_c is not exact. From Eq. (2.24), we have [28]

$$(C_v)_{max} \sim L^{\alpha/\nu}, \quad (2.58a)$$

$$\chi_{max} \sim L^{\gamma/\nu}. \quad (2.58b)$$

The pseudo critical point of the order parameter is not so clear that it is hard to find the critical exponent similarly. And take $t = (T - T_c)/T_c \approx K_c(K_c - K)$ into (2.23),

$$T_c(L) - T_c \sim L^{-1/\nu}, \quad (2.59a)$$

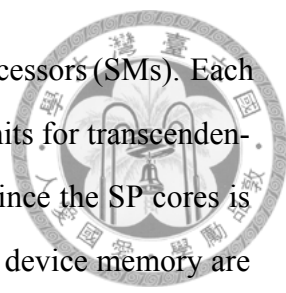
$$K_c(L) - K_c \sim L^{-1/\nu}. \quad (2.59b)$$

From above equations one can extract the critical exponents and critical temperatures from different quantities [21, 24, 28, 31, 32].

2.7 GPU

2.7.1 GPU architecture

Nowadays the existence of multicore Central Processing Units (CPUs) and manycore Graphics Processing Units (GPUs) means that the processor chips are parallel system now. This implies the parallel algorithm is now a widely applicable tool for programming. CUDA is a parallel programming model applicable to GPUs' calculations as an extension of C language developed by NVIDIA.



A GPU device consists of many multithreaded Streaming Multiprocessors (SMs). Each SM consists of many Scalar Processor (SP) cores, special function units for transcendentals, a multithreaded instruction unit, and on-chip shared memory. Since the SP cores is not as powerful as CPU cores and the sizes of the share memory and device memory are limited if they are compare to a CPU device. So how to design the level of parallelism and the memory allocation is the most important thing when doing the CUDA programming [33].

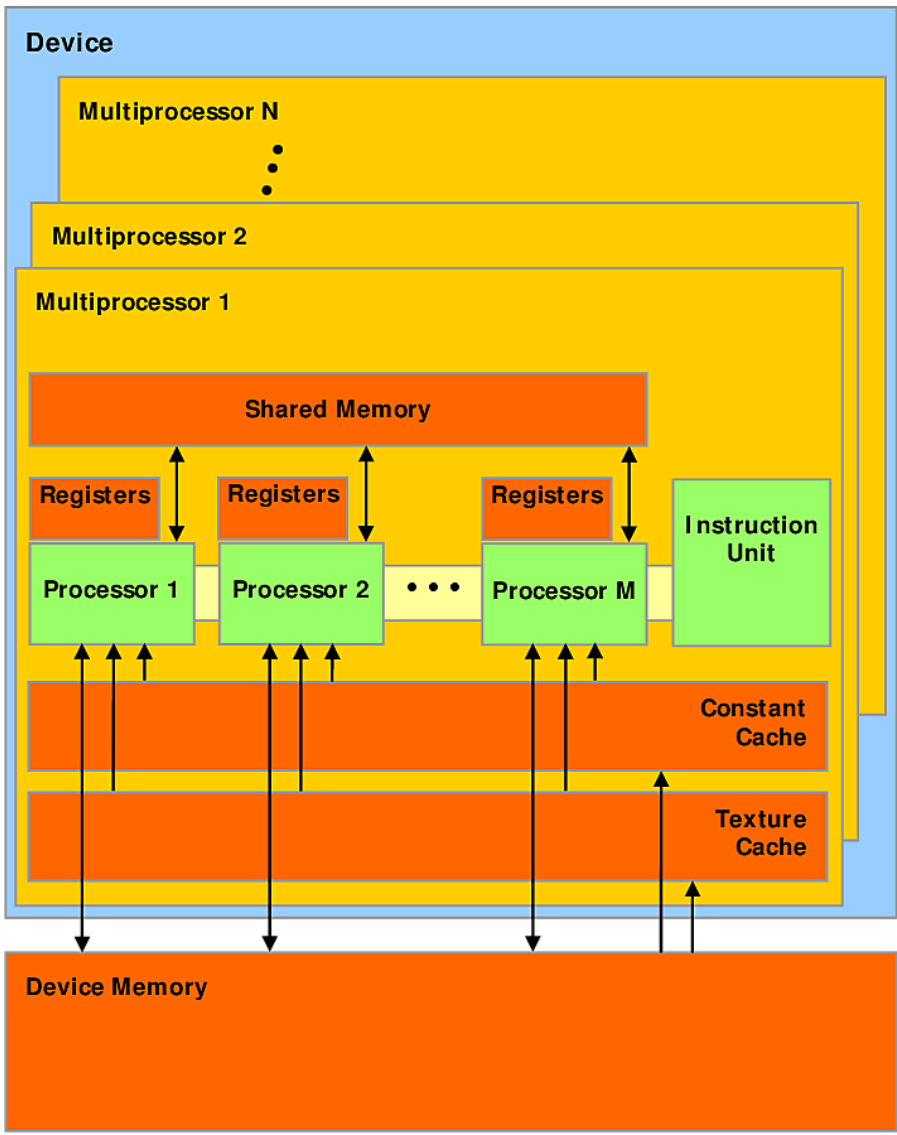
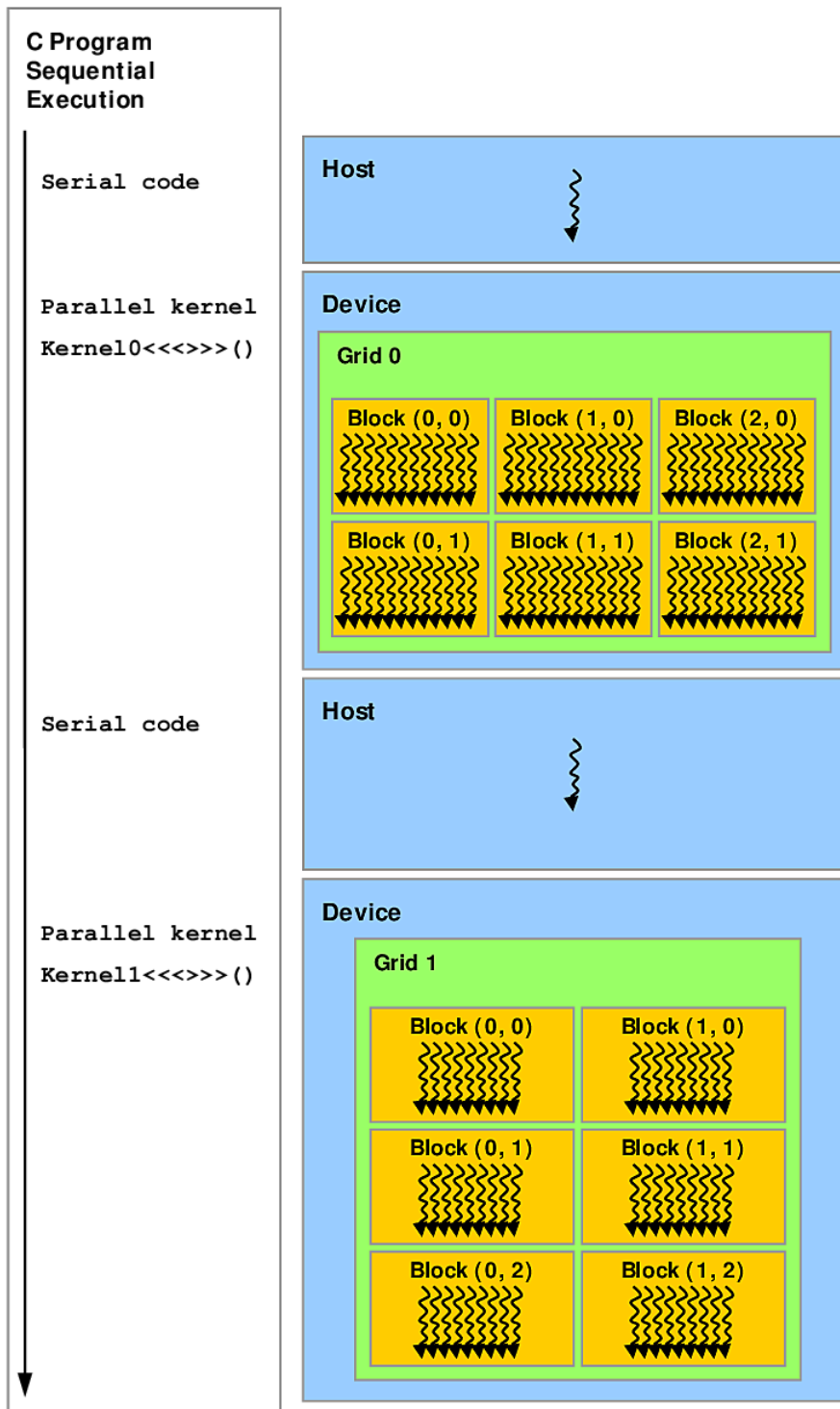
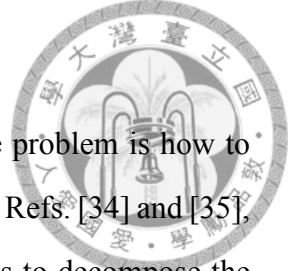


Figure 2.8: GPU hardware model. [33]



Serial code executes on the host while parallel code executes on the device.

Figure 2.9: A sample of programming with GPUs. [33]



2.7.2 Algorithm of $J_1 - J_2$ Ising model on GPU

Since we can use the CUDA language to program on GPUs, the problem is how to parallelize the MC simulation on GPUs. Our algorithm is based on the Refs. [34] and [35], the 2D and 3D Monte Carlo simulations on GPUs. The basic idea is to decompose the system lattice into numbers of sublattices which the spins in the same sublattice are not interacting with each others so one can update them in the same time [34, 35]. We use the checkerboards [21] in Fig. 2.10 to do the parallelism. To finish one MCS, we first update all spins in one sublattice on numbers of threads and then update those in another one and so on until all spins are updated. Note that the $J_1 - J_2$ Ising model also include the classical Ising model for $g = 0$, we update the spins in the sublattices in sequence $\{1, 4, 2, 3\}$ to make sure it can also work in the classical Ising system.

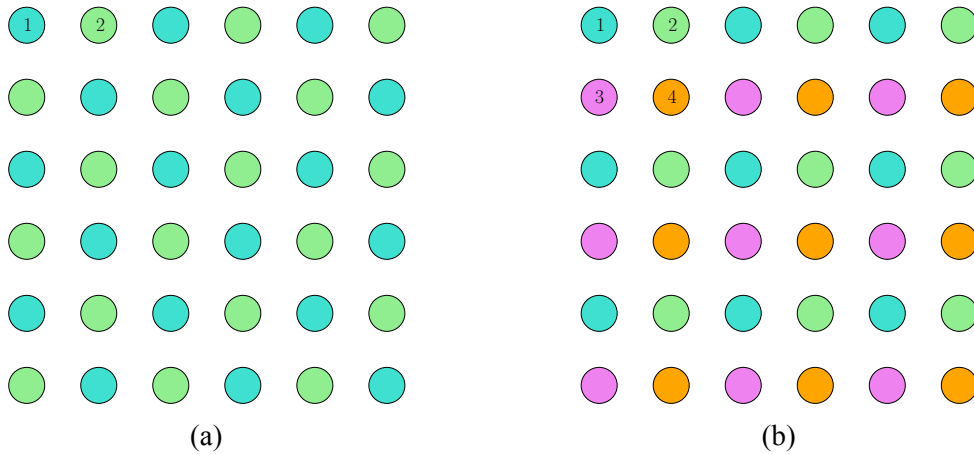


Figure 2.10: Fig. (a) shows the checkerboard decomposition of classical Ising model on a square lattice [21, 34]. Fig. (b) shows the checkerboard decomposition of $J_1 - J_2$ Ising model on a square lattice [21]. The spins in same color means the spins are in the same sublattice, which are not interacting to each others. To finish one MCS, one should update all spins in one sublattice then those in another one and so on until all spins are updated.



Chapter 3

Results

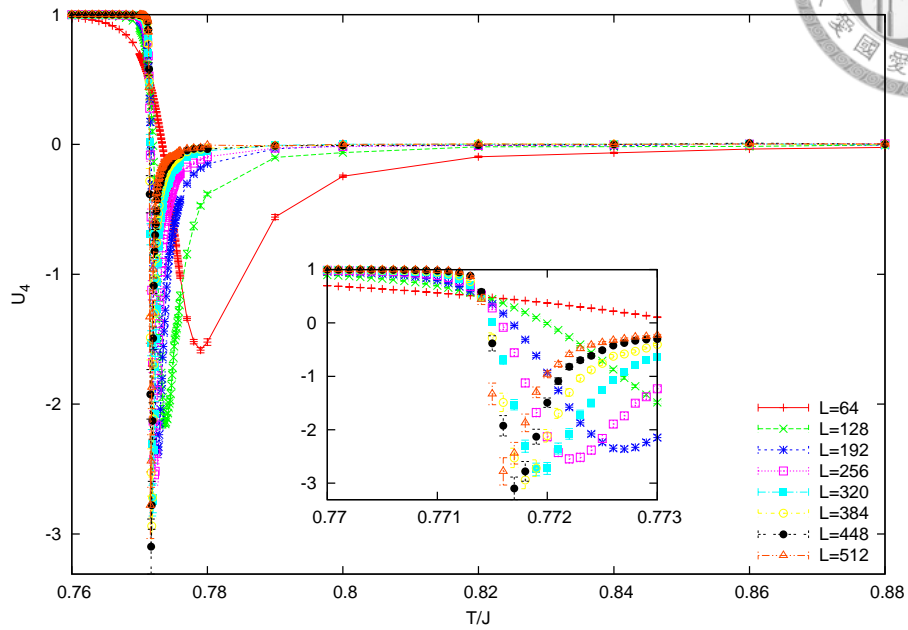
3.1 Critical temperatures and critical exponents

In Sec. 2.2, we have referred that there are continuous phase transitions in both $0 \leq g < 0.5$, the Ising-like transition [1–10], and $g > g^*$ with $g^* \approx 0.67$, the AT-like transition [1, 2]. There exists a the weak first-order phase transitions are in the range $0.5 < g < g^*$ [1–4].

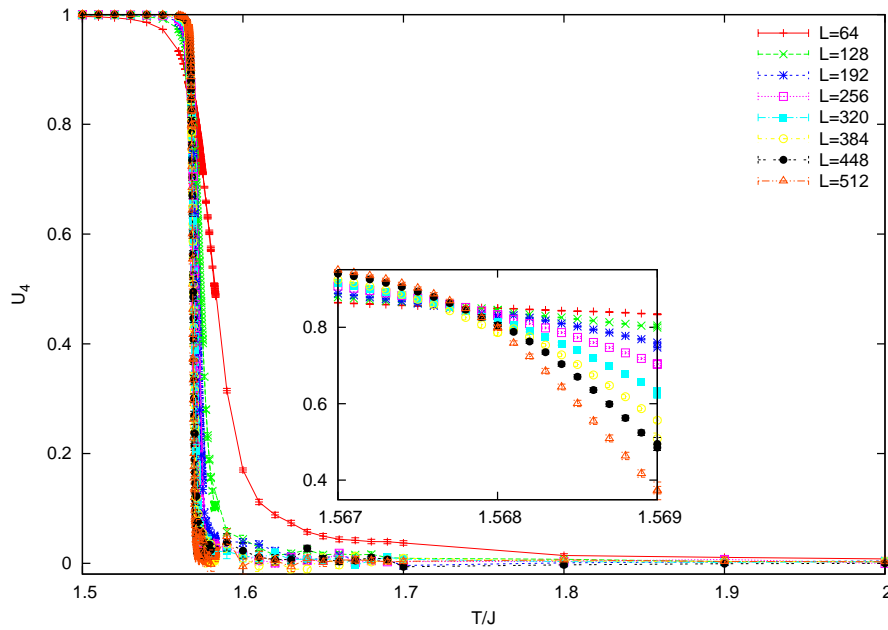
First we want to obtain the critical temperatures. The critical temperatures of continuous phase transitions can be retrieved by finite-size scaling and the crossing of the Binder cumulants at different size. For a first-order phase transition, we can not get the critical temperature easily just similar to a continuous phase transition. Here we want to study the case of the weak first-order phase transition, and the critical temperatures extracted from the finite-size scaling and the Binder cumulant are good estimates of the critical temperatures [36].

Then we use the finite-size scaling to extract the critical exponents and critical temperatures for each g . Here we use three different quantities in Eq. (2.55) to extract ν . From the pseudo critical point of each size and use Eq. (2.59), we can extract the critical temperatures, here we just show the part of the results because they are similar to each other.

After we know the values of ν , we can extract the other exponents by other scaling relations. Note that the scaling function of specific heat, Eq. (2.27a) is only valid for α is



(a) $g = 0.55$



(b) $g = 0.80$

Figure 3.1: Binder cumulants for both first-order and continuous phase transitions. The figures show the crossing points of each size which refer to the critical temperatures. In (a) the property of the first-order phase transition is dominated, a negative peak grow as size increase. And the Binder cumulants of each size cross roughly at one point because it is the weak first-order transition [36].

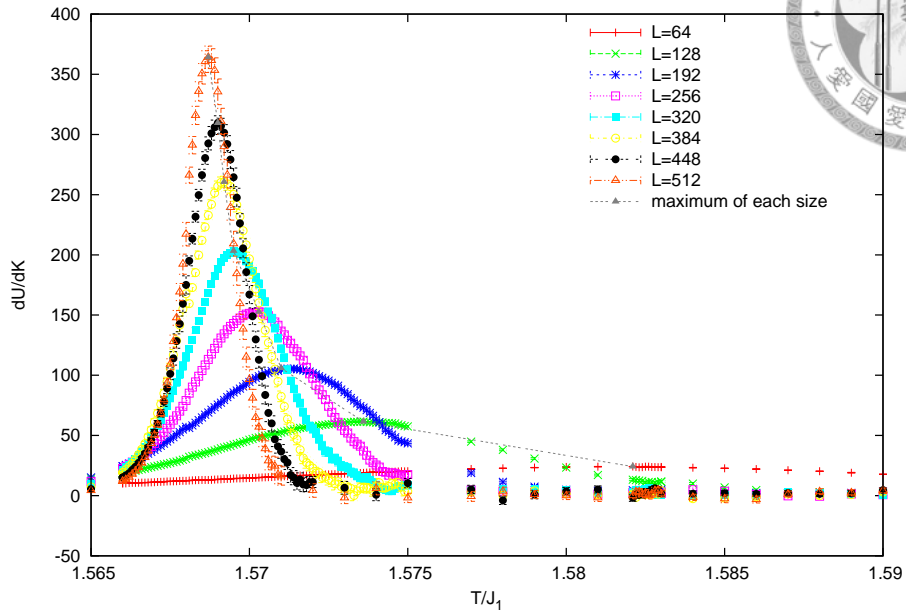


Figure 3.2: Use Eq. (2.56) to calculate $\delta U/\delta K$ then find the maximum and the pseudo critical temperature of each size.

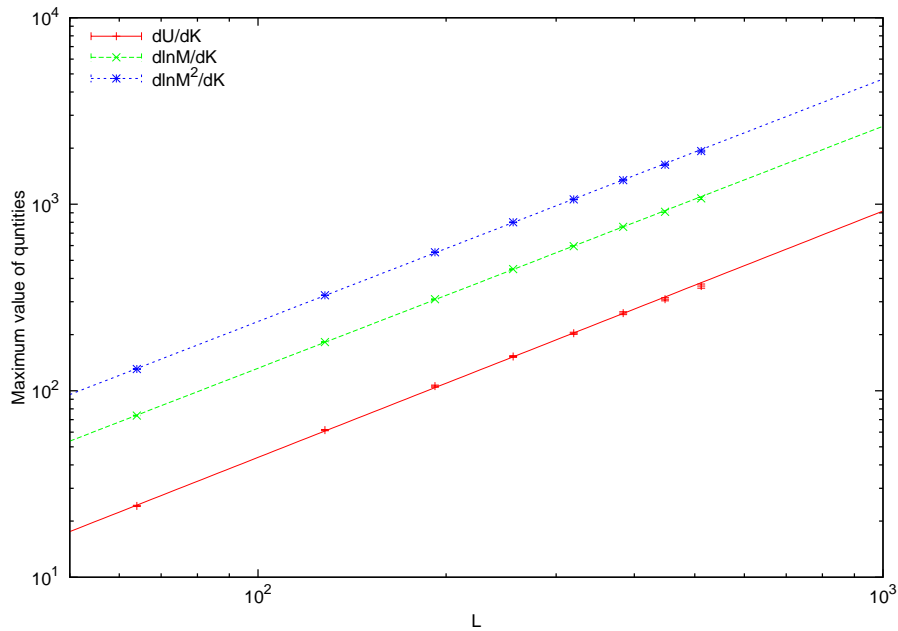


Figure 3.3: Use the quantity $Q_{max} \sim L^{1/\nu}$ to find the slopes of best fitting lines, we extract the value of ν are 0.7706(2), 0.7691(2) and 0.7570(5) from Eq. (2.55a), (2.55b) and (2.55c) for $g = 0.8$.

positive, and the specific heat is a sensitive quantity so that the simple applications in Eq. (2.58a) and Eq. (2.57a) is not applicable to many cases. For $\alpha \leq 0$, the specific heat still have a weak, logarithmic divergence. When α is closed to 0, or g is closed to g^* (the Potts point), the scaling of the specific heat should consider subleading corrections [2, 11; 37, 38]. Since we do not know when we should take the correction terms into account, here we just show the exponents using Eq. (2.58a) and Eq. (2.57a). And the real α 's are calculated by scaling relation in (2.28b) and ν 's.

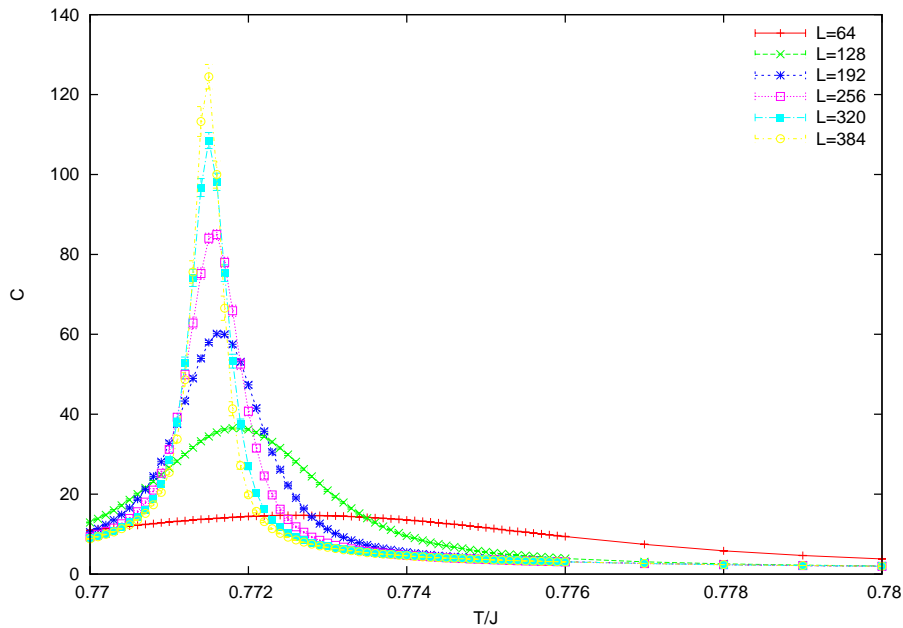
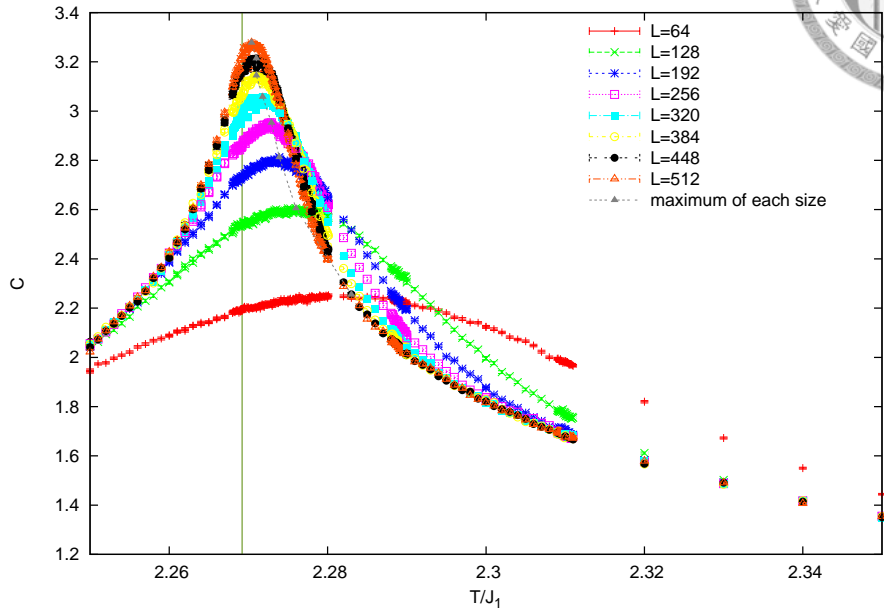


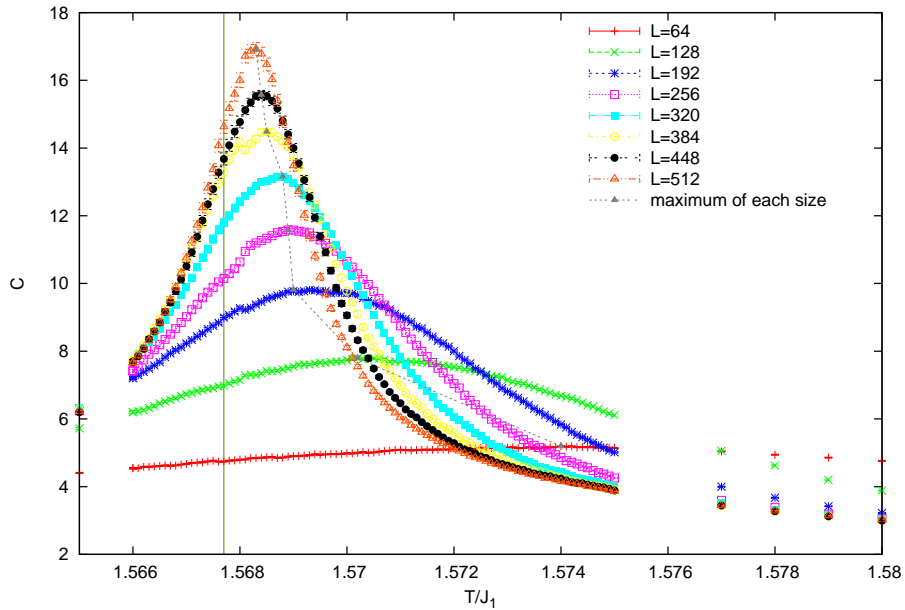
Figure 3.4: Figure shows one feature of the weak first-order transition for $g = 0.55$, the L logarithmic dependence $C_{max} \sim L^c$, here $c > 1$ and c should close to d (number of the dimensions of the system) when L is large enough.

Since the order parameter have no obvious extreme behaviour, it is hard to find the pseudo critical temperature of each size. The exponent β can be extracted by the order parameter at critical temperature of each size in Eq. (2.57b) or be calculated from scaling relations in (2.28). Note that we do not have all the exact values of critical temperatures, they may have the error up to 2×10^{-4} for some g , and it cause the errors of the extracted values of β/ν 's about 10%.

We also extract γ from susceptibility using Eq. (2.58b) and Eq. (2.57c). Since susceptibility is a stable quantity, we use γ as a basic exponent just like ν to calculate the other exponents using scaling relations.



(a) $g = 0$



(b) $g = 0.8$

Figure 3.5: Figure (a) shows the specific heat of each size in a classical square Ising lattice, $\alpha/\nu = 0$ from exact solutions. But one can easily find out the specific heat still have a logarithmic divergence of size, $C_{max}(L) \sim L^k$ and $k \approx 0.18$. In (b) we use the scaling laws in Eq. (2.57a) and Eq. (2.58a), the extracted values of α are 0.434(5) and 0.437(4) for $g = 0.8$.

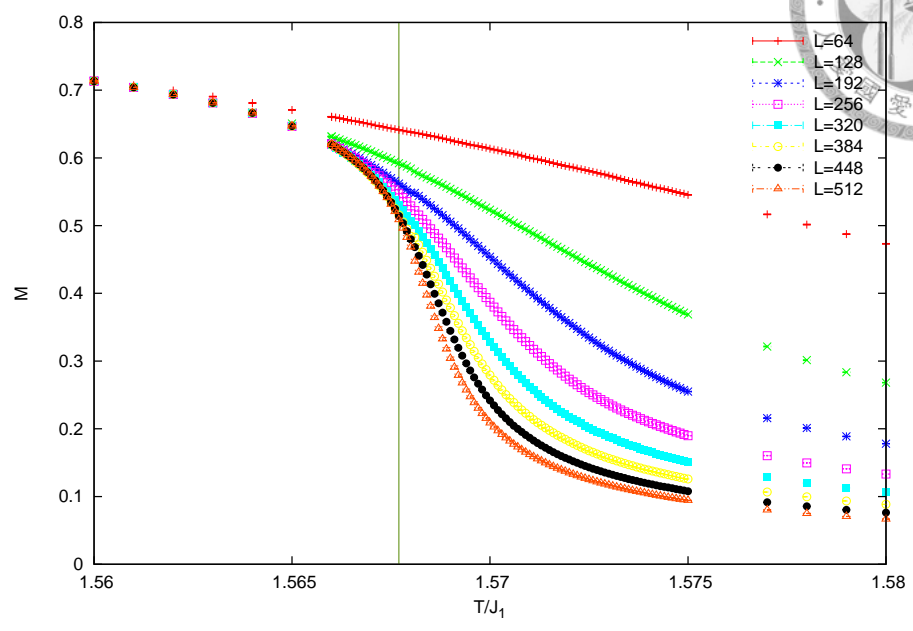
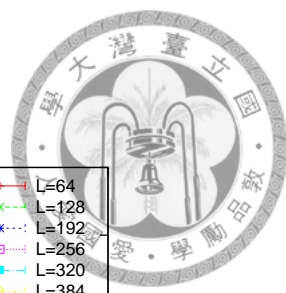


Figure 3.6: $\beta/\nu = 0.120(4)$ using Eq. (2.57b) for $g = 0.8$.

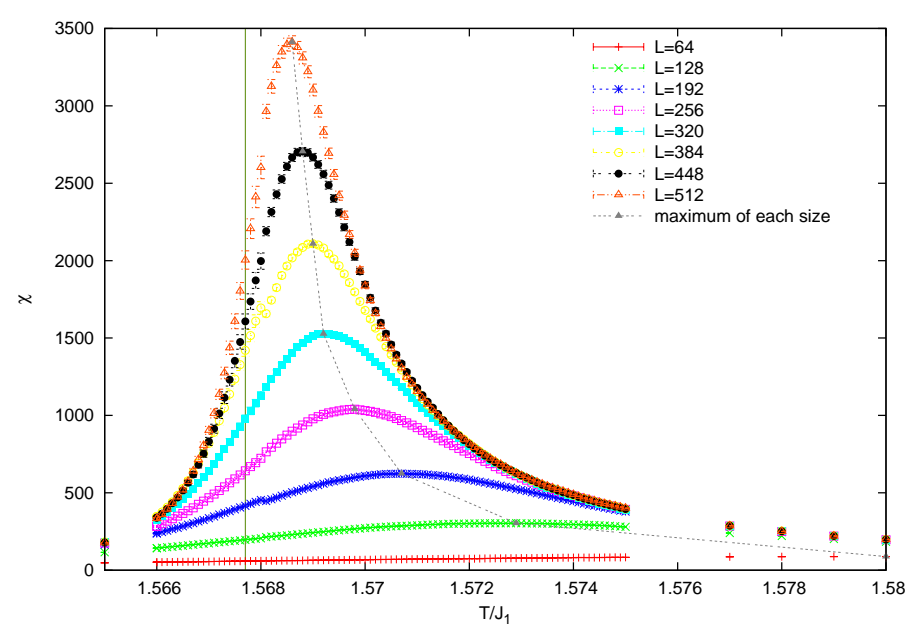


Figure 3.7: The extracted values of γ/ν are $1.736(2)$ and $1.7685(6)$ from Eq. (2.57c) and Eq. (2.58b) for $g = 0.8$.

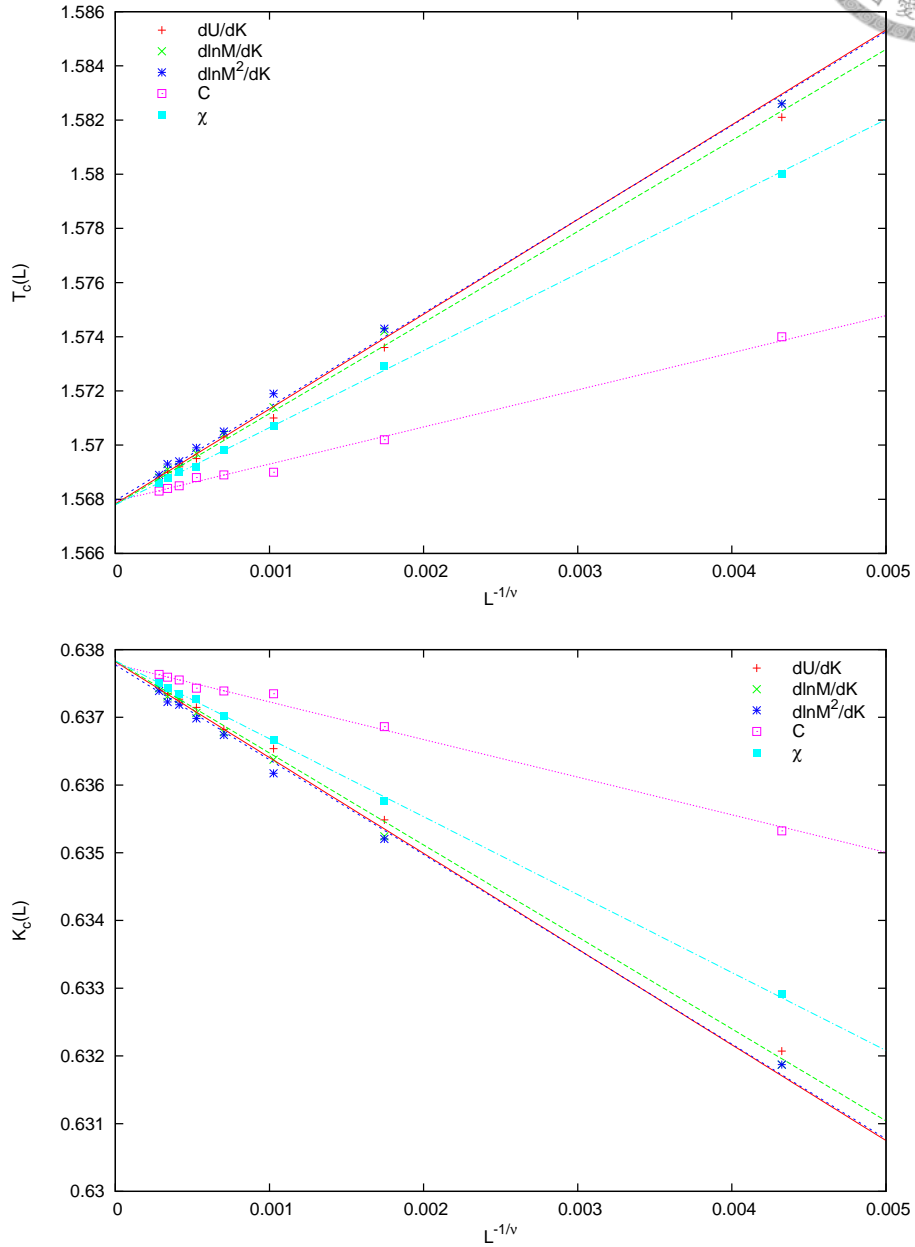
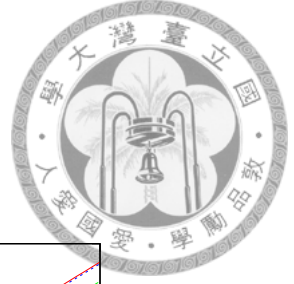


Figure 3.8: Figure (a) shows the pseudo critical temperatures of each quantities of each size, using Eq. (2.59a) to find out critical temperature. Figure (b) is similar to (a), just change T_c to K_c and use Eq. (2.59b). The values of critical temperatures are 1.57(3), 1.568(6), 1.568(8), 1.57(1) and 1.568(9) from C_{max} , X_{max} , $(\delta \ln M / \delta K)_{max}$, $(\delta \ln M^2 / \delta K)_{max}$ and $(\delta U / \delta K)_{max}$ for $g = 0.8$.

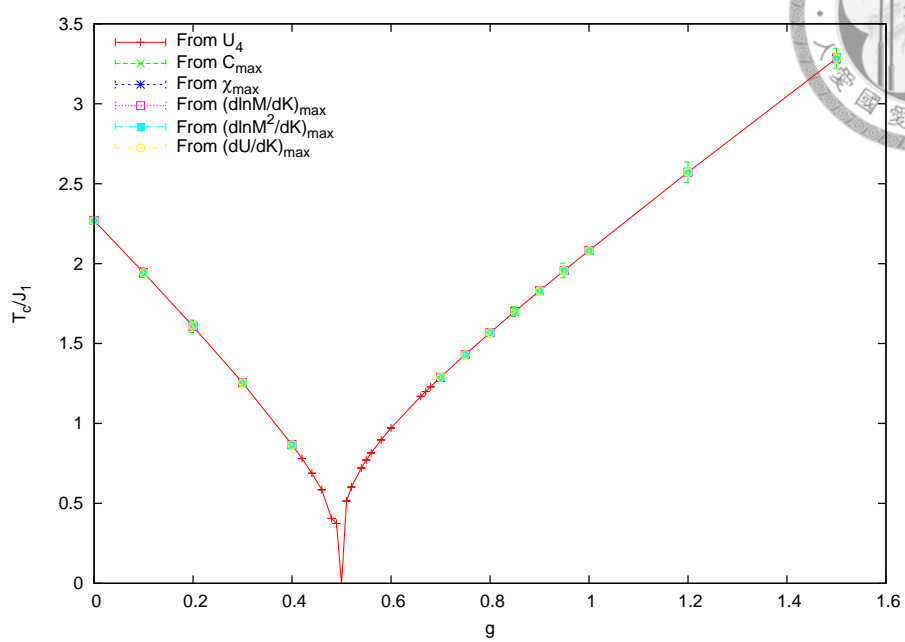
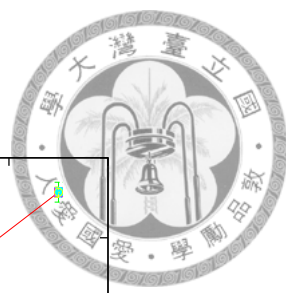


Figure 3.9: Figure shows all critical temperatures extracted from each methods for $0 \leq g \leq 1.5$.

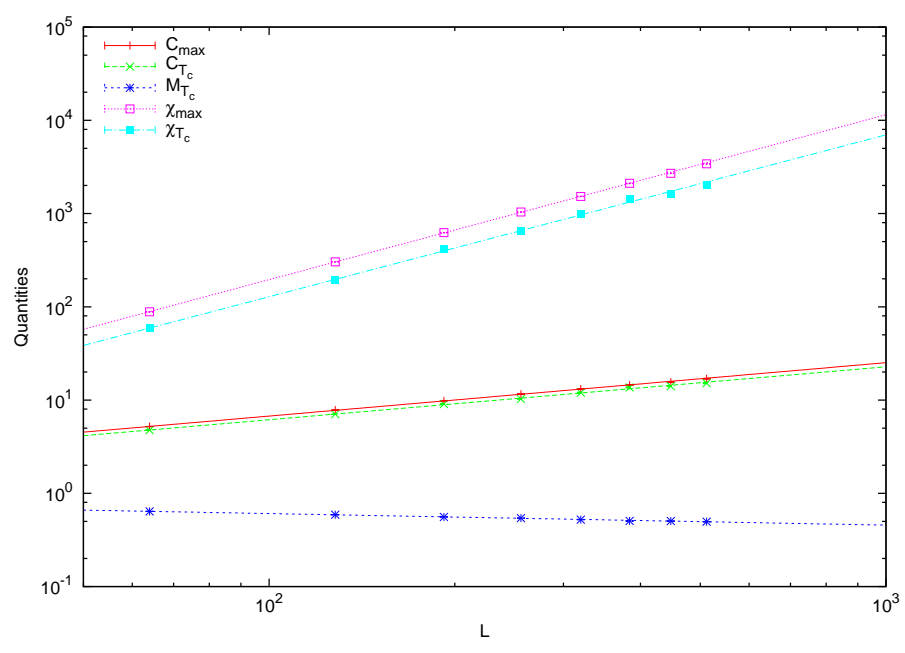


Figure 3.10: Figure shows the maximum values of each quantities, the slopes of each quantities are used to extract α/ν , β/ν and γ/ν .

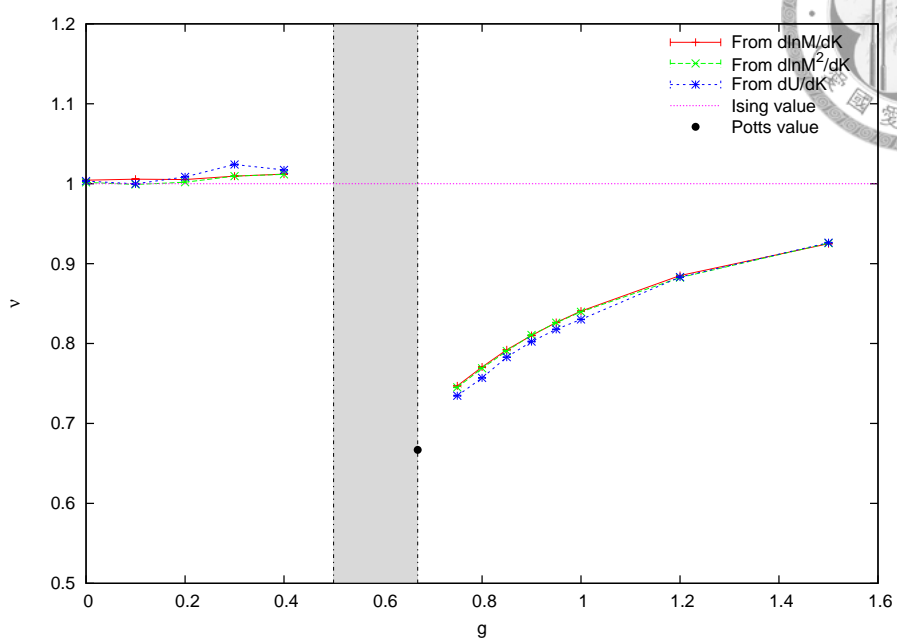


Figure 3.11: Figure shows the values of ν extracted from Eq. (2.55).

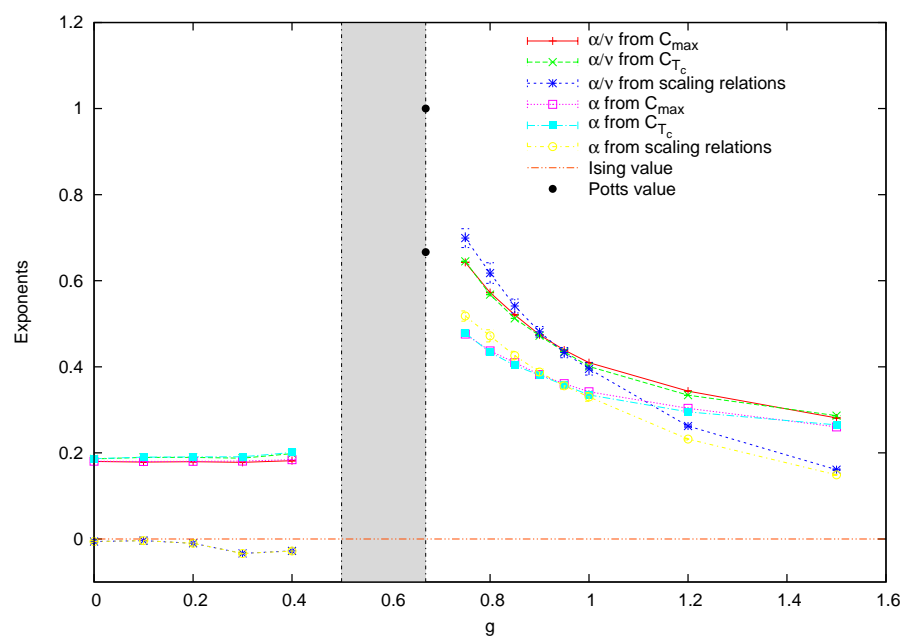


Figure 3.12: Figure shows the values of α extracted from Eq. (2.57a), (2.58a) and calculated by scaling relation (2.28b). Note that the correction of the scaling function is needed near the Potts point [2, 38] and for α/ν closed to 0 [11, 37].

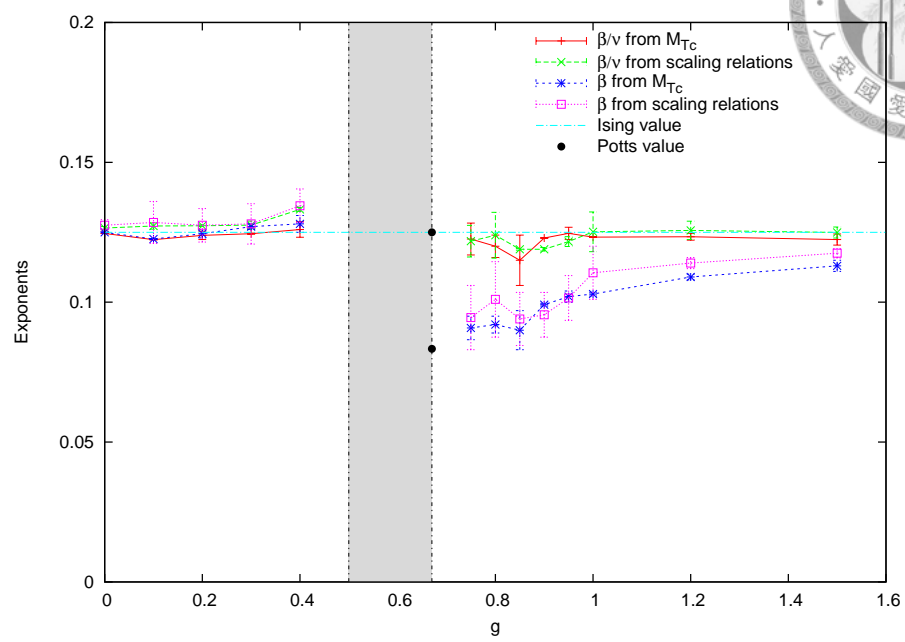
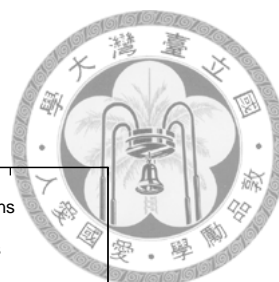


Figure 3.13: Figure shows the values of β extracted from Eq. (2.57b) and calculated by scaling relation (2.28).

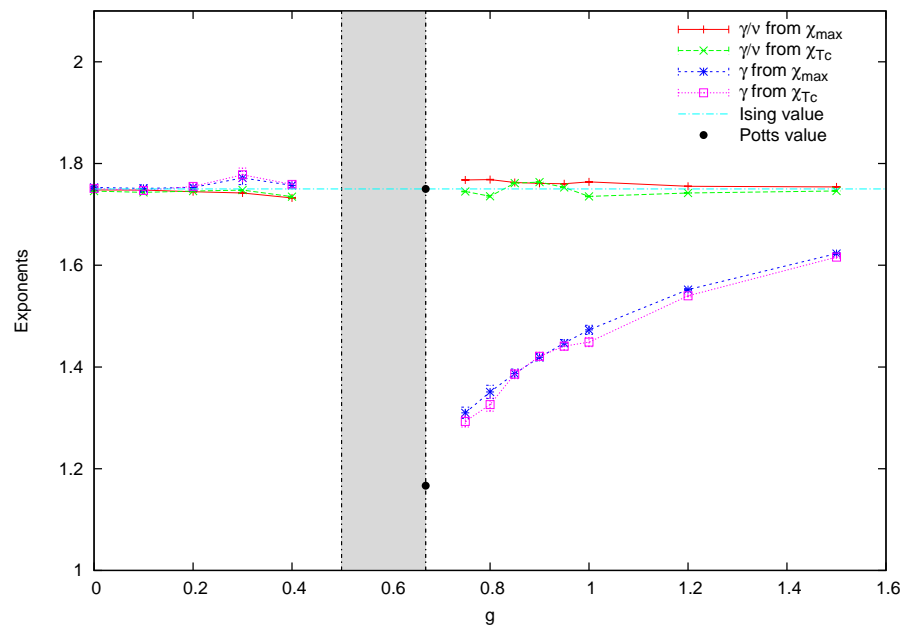
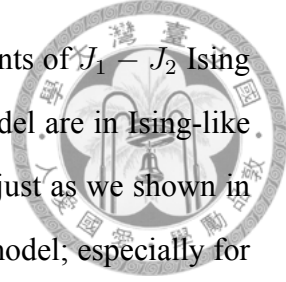


Figure 3.14: Figure shows the values of γ extracted from Eq. (2.57c) and (2.58b).

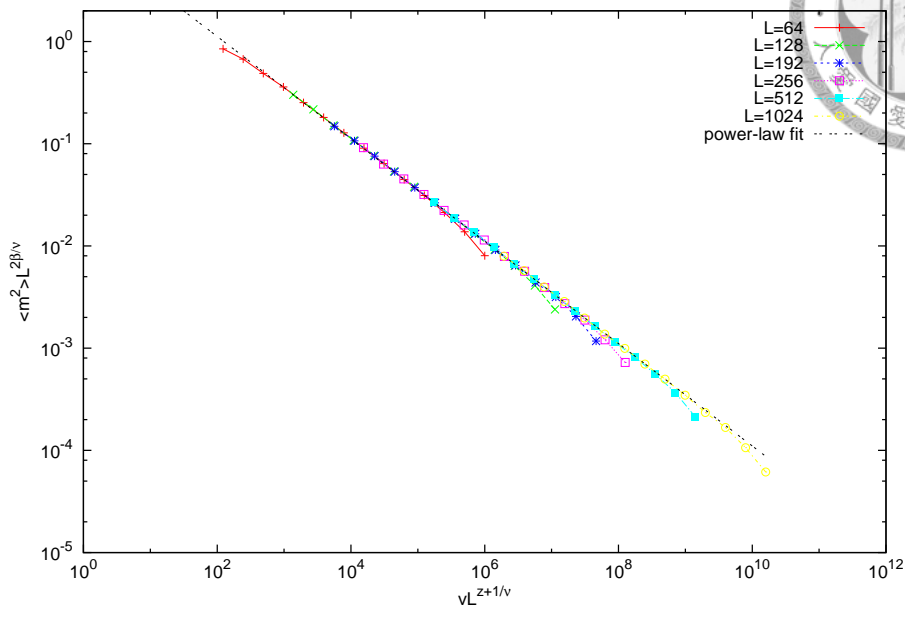
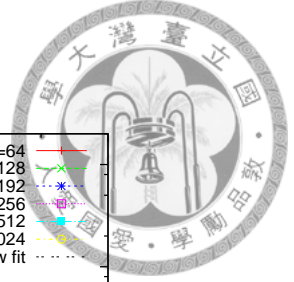


From Fig. 3.11, 3.12, 3.13 and 3.14, we show the critical exponents of $J_1 - J_2$ Ising model for different g . In the region $0 \leq g < 0.5$, $J_1 - J_2$ Ising model are in Ising-like transition, so the critical exponents are the same as the Ising values just as we shown in figures. For $g^* \leq g$, the model can be mapped to the Ashkin-Teller model; especially for $g = g^*$, it can be mapped to the 4-state Potts model. If $g \rightarrow \infty$, it goes back to the classical 2D Ising transition. In these figures, one can easily find that the values of each critical exponents are moving from Potts value to the Ising value for g increasing from Potts point to infinity.

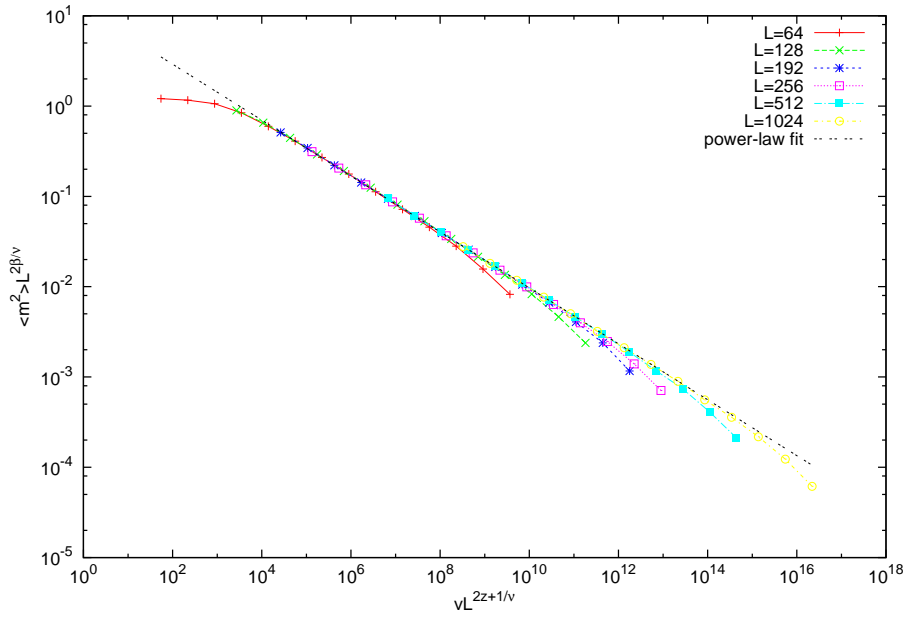
3.2 Extraction of the dynamic exponent

In this section we study the square of the order parameters of linear and non-linear quenches with Metropolis dynamics on 2D $J_1 - J_2$ Ising lattice for different g in both Ising-like and AT-like regime. We predict that the dynamic exponents of the Metropolis algorithm z in the Ising-like regime ($0 \leq g < 0.5$) is a constant because all the critical phenomena are similar for different g and z should close to the Ising value. From recent studies, we know that the dynamic exponent z is different for different dimensionality in the Ising model [39–41], and z has little difference in 3D Ising model and 3D Heisenberg model [42], which imply that z may be different for different transition types. From Refs. [43–46], we have $z \approx 2.17(1)$, which is approximately a constant for $q = 2, 3, 4$ in the Potts model (See Tab. 3.1). Since the $J_1 - J_2$ Ising model have an AT-like transition in region $g^* \leq g$, the model can be mapped to the 4-state Potts model at $g = g^*$, and it back to the Ising-like transition as $g \rightarrow \infty$, which is equivalent to the 2-state Potts transition, we predict that z is roughly a constant in the AT-like region no matter the varying g (the same as a varying K in AT model).

In Fig. 3.17, we find that the dynamic exponent of Metropolis algorithm z seems to remain a constant with varying g in both Ising-like and AT-like regimes just as we predict. It enhance the statement that z is the same value in Potts model for $q = 2, 4$, also implies that z should be a constant in AT model with different K . Our result $z = 2.17(1)$ is also match the most reliable values of z of 2D Ising transition, 2.173(4) and 2.164(3) from

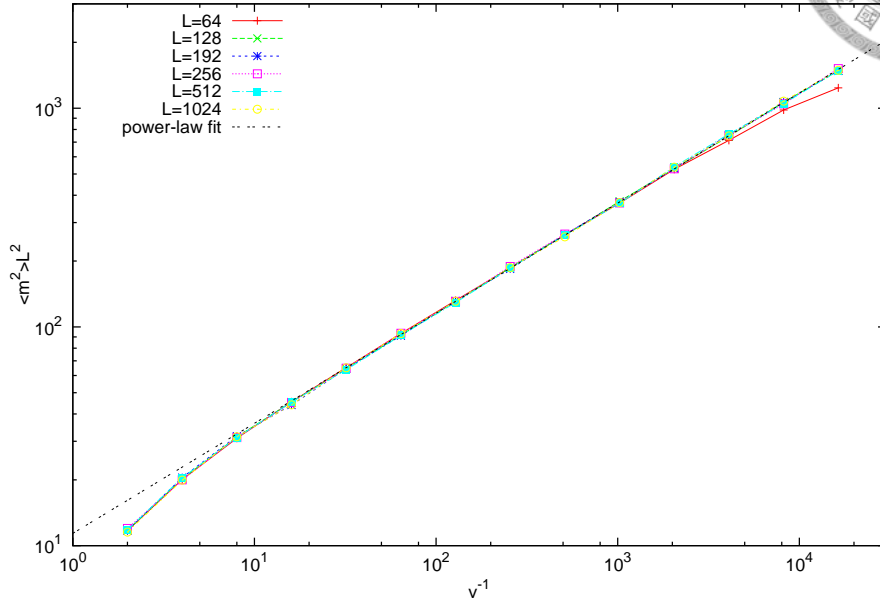
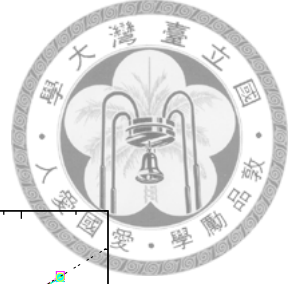


(a) A linear quench with $r = 1$ for $g = 0.8$.

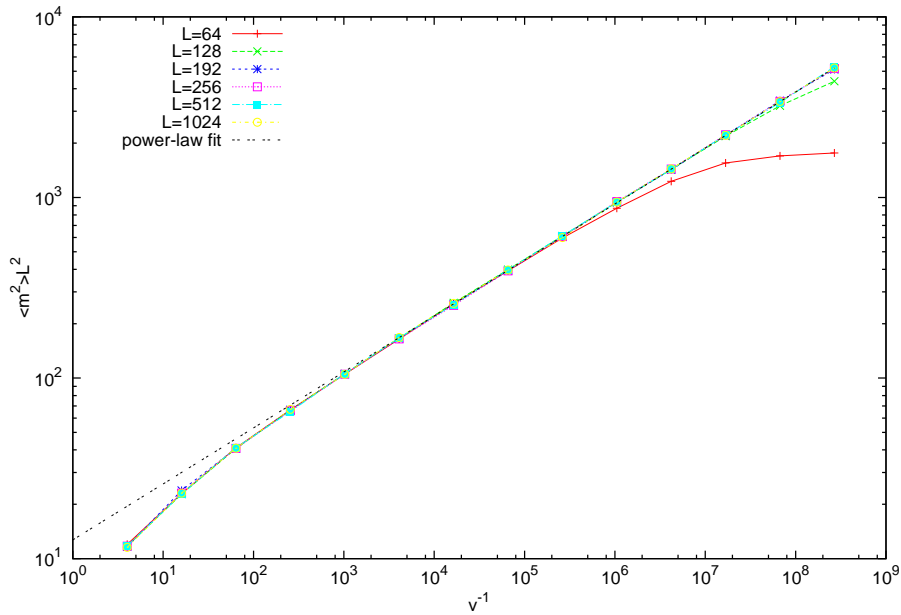


(b) A non-linear quench with $r = 2$ for $g = 0.8$.

Figure 3.15: Data collapse in linear and non-linear quenches from $T_i = 1.5T_c$ to T_c with Metropolis dynamics of 2D $J_1 - J_2$ Ising model. Use quantities in Eq. (2.42) to find the value of z . The left points out of straight line are in the quasi-adiabatic regime $v \lesssim v_{KZ}(L)$, the center points are in the universal regime $v_{KZ}(L) \ll v \ll 1$, and right most points of each L are in the diabatic regime $v \gtrsim 1$. The dash line shows the slopes expected in Eq. (2.44). The values of the extracted z 's of Metropolis algorithm are 2.18(1) and 2.17(1) for $r = 1$ and $r = 2$, separately. Note that the data-collapsing only consider the points in the universal regime.



(a) A linear quench with $r = 1$ for $g = 0.8$.



(b) A non-linear quench with $r = 2$ for $g = 0.8$.

Figure 3.16: Linear and non-linear quenches from $T_i = 1.5T_c$ to T_c with Metropolis dynamics of 2D $J_1 - J_2$ Ising model. Using the points in universal regime to extract z from relation in Eq. (2.48). The values of the extracted dynamic exponent z 's of Metropolis algorithm are 2.17(1) and 2.171(8) for $r = 1$ and $r = 2$.

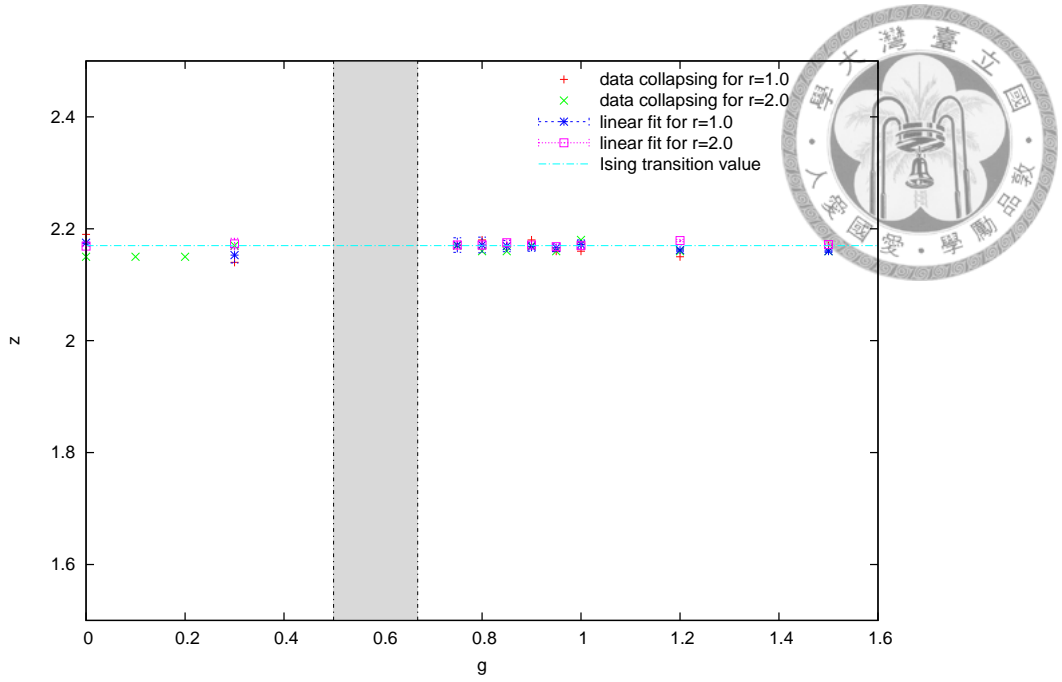


Figure 3.17: Figure shows the values of dynamic exponents z 's of Metropolis algorithm extracted for different g from Eq. (2.44) and (2.48).

Ref. [14] and Ref. [20], and it is very close to 2.16(1) which is the value of case II in the extended $J_1 - J_2$ model with vacancy order in Ref. [47] where the case is similar to the $J_1 - J_2$ Ising model with $g = 1$.

Model	z
2D Ising model [14]	2.173(4)
2D Ising model [20]	2.164(3)
$q = 2$ Potts (Ising) model [44]	2.167(2)
$q = 3$ Potts model [44]	2.174(2)
$q = 3$ Potts model [46]	2.164(7)
$q = 4$ Potts model [46]	2.16(1)
This work	2.17(1)

Table 3.1: The dynamic exponents from references.



Chapter 4

Summary and Discussion

We have shown the Ising-like transitions from Néel phase in the $J_1 - J_2$ Ising model for $0 \leq g < 1/2$, the first-order phase transitions from striped ordered phase for $1/2 \leq g < g^*$ and the AT-like phase transitions from striped ordered phase for $g^* < g$. For this model, the point $g = g^* \approx 0.67$ corresponds to the 4-state Potts transition and the transition is back to Ising (2-state Potts) transition as $g \rightarrow \infty$. We provide the critical exponents with varying g as an evidence of the transition types. The exponents of Ising-like transitions have no g -dependence. And the exponents of AT-like transitions are changing from Potts values to Ising values as g increasing from g^* to infinity, just as those in AT model.

We also perform quench dynamics of the system with Metropolis algorithm for both Ising-like and AT-like transitions. We have found that the dynamic exponent z of the Metropolis dynamic in AT-like transitions remains a constant with varying g (the same meaning as varying K in AT model.) Also, z is a constant in Ising-like transition regime for different g . And they are the same as each other and match the values from Refs. [14, 20]. The consequence makes sense because the model corresponds to the 4-state Potts transition at $g = g^*$, and is closed to the Ising-like (2-state Potts) transition as $g \rightarrow \infty$.

Our future works include the quenching with different MC methods, for instance, cluster update, we expect that it is similar to the one with Metropolis method because the differences between them are just like the differences of quench velocities. Another project is to analyze the finite-size effects and the quench dynamics of AT-like transition regime for g near the Potts point which depend on a logarithmic corrections [2, 48]. And finding


the real value of g^* is also a challenge. Moreover, there is still an open question for the transitions in the regime $1/2 < g < g^*$, especially for $g \rightarrow 1/2$, where a unusual transition occurs at $T = 0$.








Bibliography

- [1] Songbo Jin, Arnab Sen, and Anders W. Sandvik. Ashkin-teller criticality and pseudo-first-order behavior in a frustrated Ising model on the square lattice. *Physical Review Letters*, 108(4):045702, January 2012.
- [2] Songbo Jin, Arnab Sen, Wenan Guo, and Anders Sandvik. Phase transitions in the frustrated Ising model on the square lattice. *Physical Review B*, 87(14), April 2013.
- [3] A. Kalz, A. Honecker, S. Fuchs, and T. Pruschke. Phase diagram of the Ising square lattice with competing interactions. *The European Physical Journal B*, 65(4):533–537, October 2008.
- [4] Ansgar Kalz and Andreas Honecker. Location of the Potts-critical end point in the frustrated Ising model on the square lattice. *Physical Review B*, 86(13), October 2012.
- [5] Lars Onsager. Crystal statistics. i. a two-dimensional model with an order-disorder transition. *Physical Review*, 65(3-4):117–149, February 1944.
- [6] M. P. Nightingale. Non-universality for Ising-like spin systems. *Physics Letters A*, 59(6):486–488, January 1977.
- [7] Robert H. Swendsen and Samuel Krinsky. Monte Carlo renormalization group and Ising models with $n > 2$. *Physical Review Letters*, 43(3):177–180, July 1979.
- [8] J. Oitmaa. The square-lattice Ising model with first and second neighbour interactions. *Journal of Physics A: Mathematical and General*, 14(5):1159, May 1981.

- 
- [9] K. Binder and D. P. Landau. Phase diagrams and critical behavior in Ising square lattices with nearest- and next-nearest-neighbor interactions. *Physical Review B*, 21(5):1941–1962, March 1980.
- [10] D. P. Landau. Phase transitions in the Ising square lattice with next-nearest-neighbor interactions. *Physical Review B*, 21(3):1285–1297, February 1980.
- [11] Anders W. Sandvik. Computational studies of quantum spin systems. *arXiv: 1101.3281 [cond-mat, physics:hep-lat]*, pages 135–338, 2010. arXiv: 1101.3281.
- [12] Kurt Binder and Dieter W. Heermann. *Monte Carlo Simulation in Statistical Physics*, volume 0 of *Graduate Texts in Physics*. Springer Berlin Heidelberg, Berlin, Heidelberg, 2010.
- [13] Leo P. Kadanoff. *Statistical Physics: Statics, Dynamics and Renormalization*. World Scientific Pub Co Inc, Singapore ; River Edge, N.J, July 2000.
- [14] Cheng-Wei Liu, Anatoli Polkovnikov, and Anders W. Sandvik. Dynamic scaling at classical phase transitions approached through nonequilibrium quenching. *Physical Review B*, 89(5):054307, 2014.
- [15] Seiji Miyashita and Hiroshi Takano. Dynamical nature of the phase transition of the two-dimensional kinetic Ising model. *Progress of Theoretical Physics*, 73(5): 1122–1140, May 1985.
- [16] S. Wansleben and D. P. Landau. Dynamical critical exponent of the 3d Ising model. *Journal of Applied Physics*, 61(8):3968–3970, April 1987.
- [17] Jacek Dziarmaga. Dynamics of a quantum phase transition and relaxation to a steady state. *Advances in Physics*, 59(6):1063–1189, November 2010.
- [18] Anatoli Polkovnikov, Krishnendu Sengupta, Alessandro Silva, and Mukund Venkatacharya. Colloquium: Nonequilibrium dynamics of closed interacting quantum systems. *Reviews of Modern Physics*, 83(3):863–883, August 2011.

- 
- [19] Fan Zhong. Finite-time scaling and its applications to continuous phase transitions. *Applications of Monte Carlo method in science and engineering. Intech (Online)*, page 469–493, 2011.
- [20] M. P. Nightingale and H. W. J. Blöte. Monte Carlo computation of correlation times of independent relaxation modes at criticality. *Physical Review B*, 62(2):1089, 2000.
- [21] David P. Landau and Kurt Binder. *A Guide to Monte Carlo Simulations in Statistical Physics*. Cambridge University Press, September 2009.
- [22] Kerson Huang. *Introduction to Statistical Physics*. CRC Press, September 2001.
- [23] Helmut G. Katzgraber. Introduction to Monte Carlo methods. *arXiv:0905.1629 [cond-mat, physics:physics]*, May 2009. arXiv: 0905.1629.
- [24] Junqi Yin and D. P. Landau. Phase diagram and critical behavior of the square-lattice Ising model with competing nearest-neighbor and next-nearest-neighbor interactions. *Physical Review E*, 80(5):051117, November 2009.
- [25] K. Binder. Critical properties from Monte Carlo coarse graining and renormalization. *Physical Review Letters*, 47(9):693–696, August 1981.
- [26] K. Binder and D. P. Landau. Finite-size scaling at first-order phase transitions. *Physical Review B*, 30(3):1477–1485, August 1984.
- [27] John Cardy. *Scaling and Renormalization in Statistical Physics*. Cambridge University Press, Cambridge ; New York, April 1996.
- [28] P. Peczak, Alan M. Ferrenberg, and D. P. Landau. High-accuracy Monte Carlo study of the three-dimensional classical Heisenberg ferromagnet. *Physical Review B*, 43(7):6087, 1991.
- [29] T. W. B. Kibble. Topology of cosmic domains and strings. *Journal of Physics A: Mathematical and General*, 9(8):1387, August 1976.

- 
- [30] W. H. Zurek. Cosmological experiments in superfluid helium. *Nature*, 317(6037):505–508, October 1985.
- [31] Alan M. Ferrenberg and D. P. Landau. Critical behavior of the three-dimensional Ising model: A high-resolution Monte Carlo study. *Physical Review B*, 44(10):5081–5091, September 1991.
- [32] Kun Chen, Alan M. Ferrenberg, and D. P. Landau. Static critical behavior of three-dimensional classical Heisenberg models: A high-resolution Monte Carlo study. *Physical Review B*, 48(5):3249–3256, August 1993.
- [33] CUDA C programming guide.
- [34] Tobias Preis, Peter Virnau, Wolfgang Paul, and Johannes J. Schneider. GPU accelerated Monte Carlo simulation of the 2d and 3d Ising model. *Journal of Computational Physics*, 228(12):4468–4477, July 2009.
- [35] Benjamin Block, Peter Virnau, and Tobias Preis. Multi-GPU accelerated multi-spin Monte Carlo simulations of the 2d Ising model. *Computer Physics Communications*, 181(9):1549–1556, September 2010.
- [36] L. Schülke and B. Zheng. Dynamic approach to weak first-order phase transitions. *Physical Review E*, 62(5):7482, 2000.
- [37] V. Privman and J. Rudnick. Systems with logarithmic specific heat: finite-size scaling. *Journal of Physics A: Mathematical and General*, 19(18):L1215, 1986.
- [38] Jesus Salas and Alan D. Sokal. Logarithmic corrections and finite-size scaling in the two-dimensional 4-state Potts model. *Journal of statistical physics*, 88(3-4):567–615, 1997.
- [39] Z. Alexandrowicz. Description of critical dynamics by static geometry of clusters. *Physica A: Statistical Mechanics and its Applications*, 189(1–2):148–159, October 1992.

- 
- [40] G. P. Zheng and J. X. Zhang. Determination of dynamical critical exponents from hysteresis scaling. *Physical Review E*, 58(2):R1187, 1998.
- [41] Mehmet Dilaver, Semra Gündüç, Meral Aydın, and Yiğit Gündüç. A new approach to dynamic finite-size scaling. *International Journal of Modern Physics C*, 14(07): 945–954, 2003.
- [42] Ibragimkhan Kamilovich Kamilov, Akai Kurbanovich Murtazaev, and Kh K. Aliev. Monte Carlo studies of phase transitions and critical phenomena. *Physics-Uspekhi*, 42(7):689–709, 1999.
- [43] S. Tang and D. P. Landau. Monte Carlo study of dynamic universality in two-dimensional Potts models. *Physical Review B*, 36(1):567, 1987.
- [44] Keekwon Nam, Bongsoo Kim, and Sung Jong Lee. Nonequilibrium critical relaxation of the order parameter and energy in the two-dimensional ferromagnetic Potts model. *Physical Review E*, 77(5), May 2008.
- [45] Shuangli Fan and Fan Zhong. Determination of the dynamic and static critical exponents of the two-dimensional three-state Potts model using linearly varying temperature. *Physical Review E*, 76(4), October 2007.
- [46] Xianzhi Huang, Shurong Gong, Fan Zhong, and Shuangli Fan. Finite-time scaling via linear driving: Application to the two-dimensional Potts model. *Physical Review E*, 81(4), April 2010.
- [47] N. Zhou, B. Zheng, and J. Dai. Dynamic approach to finite-temperature magnetic phase transitions in the extended $J_1 - J_2$ model with vacancy order. *Physical Review E*, 87(2), February 2013.
- [48] Christian Borgs and Roman Kotecký. A rigorous theory of finite-size scaling at first-order phase transitions. *Journal of statistical physics*, 61(1-2):79–119, 1990.